and use of the laser flash apparatus and R. S. Herrick for communication of unpublished results.

Registry No. 1A, 12093-91-3; **1B**, 64494-50-4; **2A**, 117098-27-8; **2B**, 117098-28-9; **3A**, 117098-24-5; **3B**, 117098-25-6; (*SR*):(*RS*)-**4**, 104832-41-9; (*RR*):(*SS*)-**4**, 113350-82-6; (*SR*):(*RS*)-**5**, 113215-01-3; (*RR*):(*SS*)-**5**, 113109-99-2; **8**, 33135-99-8; **9**, 117098-26-7.

Supplementary Material Available: Kinetic data and plots for trapping **3B** with $P(C_2H_5)_3$ and $P(C_6H_5)_3$ and **3A** with $P(C_6H_5)_3$ and UV/vis spectrum of **1A** (10 pages). Ordering information is given on any current masthead page.

Hexaisopropoxyditungsten and Dodecaisopropoxytetratungsten: $W_2(O\text{-}i\text{-}Pr)_6$ and $W_4(O\text{-}i\text{-}Pr)_{12}$. 2.[1] Studies of Cluster Dynamics and the Equilibrium between the 12-Electron Cluster and Two Metal–Metal Triple Bonds. A Symmetry-Allowed $[\pi^2_s + \pi^2_s]$ Cycloaddition Reaction and Comparisons with the Chemistry of Cyclobutadiene[2]

Malcolm H. Chisholm,* David L. Clark, and Mark J. Hampden-Smith

Contribution from the Department of Chemistry, Indiana University, Bloomington, Indiana 47405. *Received March 21, 1988*

Abstract: In toluene-d_8, the C_{2h}-rhomboidal 12-electron cluster $W_4(O\text{-}i\text{-}Pr)_{12}$ is shown to undergo a dynamic process on the NMR time scale, E_{Act} ca. 15 kcal mol^{-1}, in which the W–W double and single bonds migrate around the W_4 ring. A symmetrical rhombus, D_{2h}-$W_4(\mu\text{-}O)_4(O)_8$, is the transient structure. This motion of the metal atoms is coupled with a *correlated rotation* [Mislow, K. *Acc. Chem. Res.* **1976**, *9*, 26] about the W–O bonds of the O-*i*-Pr ligands attached to the wingtip W atoms such that proximal and distal W–O-*i*-Pr group exchange occurs. The combined motions are called the *Bloomington Shuffle* and do not involve the backbone W atoms and their attendant O-*i*-Pr ligands. A square, D_{4h}-$W_4(\mu\text{-}O)_4(O)_8$ transition state is not involved. The *Bloomington Shuffle* and the equilibrium between $W_4(O\text{-}i\text{-}Pr)_{12}$ and $2W_2(O\text{-}i\text{-}Pr)_6$ bring about a metathesis of the tungsten atoms of the W≡W bond in $W_2(O\text{-}i\text{-}Pr)_6$. The equilibrium $W_4(O\text{-}i\text{-}Pr)_{12} = 2W_2(O\text{-}i\text{-}Pr)_6$ has been studied as a function of temperature (23 to +44 °C) leading to a determination of the thermodynamic parameters $\Delta H° = +21$ (2) kcal mol^{-1} and $\Delta S° = +61$ (6) eu. The approach to equilibrium in toluene-d_8 has also been studied as a function of six temperatures in the range +23 to +44 °C starting from both $W_4(O\text{-}i\text{-}Pr)_{12}$ and $W_2(O\text{-}i\text{-}Pr)_6$. Analyses of the kinetic data reveal the activation parameters (i) for $W_4 \rightarrow 2W_2$, $\Delta H^‡ = +30$ (2) kcal mol^{-1} and $\Delta S^‡ = +18$ (6) eu, and (ii) for $2W_2 \rightarrow W_4$, $\Delta H^‡ = +10$ (1) kcal mol^{-1} and $\Delta S^‡ = -39$ (3) eu. In the coupling of two $W_2(O\text{-}i\text{-}Pr)_6$ units there is a highly ordered transition state and these results are compared to organic cycloaddition reactions. A molecular orbital analysis for the cycloreversion reaction $W_4(O\text{-}i\text{-}Pr)_{12} \rightarrow 2W_2(O\text{-}i\text{-}Pr)_6$ along a C_{2h} reaction path has been developed with the Fenske–Hall calculational method. A Walsh diagram has been constructed and an analysis of avoided crossings, real and trivial, is presented. The system is closely compared to the coupling of two ethyne molecules to give cyclobutadiene. While the latter is a symmetry-forbidden $[\pi^2_s + \pi^2_s]$ reaction in the Woodward–Hoffmann sense, the coupling of two $W_2(OH)_6$ molecules to give C_{2h}-$W_4(OH)_{12}$ is shown to be symmetry allowed.

In the previous paper[1] we described the synthesis of the first example of a metal–metal multiply bonded compound $W_2(O\text{-}i\text{-}Pr)_6(M{\equiv}M)$ and its dimer, a tetranuclear 12-electron cluster, $W_4(O\text{-}i\text{-}Pr)_{12}$. We were fortunate in obtaining a crystalline sample that contained a 1:1 mixture of the dinuclear and tetranuclear molecules in the unit cell while independent synthetic routes to each compound were established. The dinuclear compound is a member of a now extensive series of ethane-like $X_3M{\equiv}MX_3$ compounds.[3] The tetranuclear compound adopts a centrosymmetric structure in the solid state involving a central $W_4(\mu\text{-}O)_4(O)_8$ unit with virtual C_{2h} symmetry. The M_4 unit is a distorted rhombus with two short, 2.50 (1) Å, and two long, 2.73 (1) Å, M–M distances corresponding formally to W–W double and single bond distances, respectively. The preference for a distorted rhombus of metal atoms relative to a symmetrical square, D_{4h}, or rhombus, D_{2h}, having equal M–M distances, was explained as a result of a 2nd order Jahn–Teller effect. Indeed calculations on the symmetrical D_{4h} $W_4(\mu\text{-}OH)_4(OH)_8$ model compound indicate a direct analogy with cyclobutadiene.[4] In the D_{4h} (square) structure both compounds (C_4H_4 and $W_4(O\text{-}i\text{-}Pr)_{12}$) give rise to a diradical ground state. In this paper we describe our studies of the dynamic behavior of the cluster and the equilibrium, eq 1. Fascinating similarities and differences are again seen in comparing the chemistry of the M≡M and C≡C bonds of configuration $\sigma^2\pi^4$ and their 12 electron clusters.

$$W_4(O\text{-}i\text{-}Pr)_{12} \underset{k_{-1}}{\overset{k_1}{\rightleftharpoons}} 2W_2(O\text{-}i\text{-}Pr)_6 \qquad (1)$$

Results and Discussion

Cluster Dynamics. The Bloomington Shuffle. The solid-state structure of the central core of $W_4(O\text{-}i\text{-}Pr)_{12}$ is represented diagramatically in Figure 1 [where arrows at the oxygen atoms are used to define the orientation of the methine vectors]. We believe that the gross features of this structure are maintained

(1) Part 1: Chisholm, M. H.; Clark, D. L.; Folting, K.; Huffman, J. C.; Hampden-Smith, M. J. *J. Am. Chem. Soc.* **1987**, *109*, 7750.
(2) Dedicated to Professor Kurt Mislow on his retirement.
(3) Chisholm, M. H. *Angew. Chem., Intl. Ed. Engl.* **1986**, *25*, 11.
(4) For a discussion of the bonding and dynamic behavior of neutral C_4H_4 see: Davidson, E. R.; Borden, W. T. *J. Chem. Phys.* **1983**, *87*, 4783; *J. Am. Chem. Soc.* **1978**, *100*, 388; *Acc. Chem. Res.* **1981**, *14*, 69.

0002-7863/89/1511-0574$01.50/0

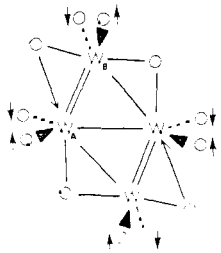

Figure 1. Schematic representation of the $W_4(\mu\text{-}O)_4(O)_8$ core of $W_4(O\text{-}i\text{-}Pr)_{12}$ with arrows indicating the orientation of the isopropoxide methine protons.

in solution, but by variable-temperature ^1H NMR spectroscopy an *intra*molecular dynamic process is clearly observed. In the solid state, $W_4(O\text{-}i\text{-}Pr)_{12}$ possesses only a center of inversion and thus six methine ^1H NMR signals might be anticipated at the low-temperature limit. However, inspection of the molecular structure in the solid state leads us to believe that the two O-*i*-Pr ligands, attached to the backbone tungsten atoms might well give rise to only one methine signal because of accidental magnetic degeneracy. The methine groups of the O-*i*-Pr ligands attached to the backbone tungsten atoms (W_A) are tangential to the cluster, i.e., at right angles to the backbone W_A–W_A axis. In contrast the terminal O-*i*-Pr ligands on the wingtip tungsten atoms (W_B) are disposed in a proximal and distal manner with respect to the cluster, which is expected to maximize the effect of the shielding anisotropy of the W_4 core (see Figures 5 and 6 in ref 1). Moreover the steric crowding at the wingtip tungsten atoms is greater because the W–O distances are shorter than those at the backbone tungsten atoms.

Variable-temperature ^1H NMR spectra of a toluene-d_8 solution of $W_4(O\text{-}i\text{-}Pr)_{12}$ and $W_2(O\text{-}i\text{-}Pr)_6$ are shown in Figure 2. Only the methine region of the spectrum is shown and we shall only discuss here the qualitative aspects of the cluster dynamics. We are at present attempting a definitive assignment of the resonances based on ultrahigh resolution ^{13}C NMR spectroscopy[5] and a variety of 2D NMR techniques.[6]

At 360 MHz and −40 °C a low-temperature limiting spectrum is reached involving five methine signals (septets) assignable to the cluster. *Note* the signals due to the methine protons of $W_2(O\text{-}i\text{-}Pr)_6$ do *not* represent an equilibrium concentration at any of the temperatures for which spectra are shown in Figure 2. The signals marked a, b, c, d, and e, assignable to the methine protons of the cluster, are in the integral ratio 1:2:1:1:1.

Upon raising the temperature to 0 °C all the signals remain sharp but the chemical shifts of the signals associated with c and d move together and above 0 °C have started to move apart (presumably having crossed). Upon raising the temperature from +10 to +35 °C the resonances a, c, d, and e all show line broadening indicative of an exchange process. Above 35 °C those signals merge into the baseline while that of b, the resonance of integral intensity 2 which we believe is assignable to the O-*i*-Pr ligands on the backbone tungsten atoms, remains sharp. At these higher temperatures equilibrium 1 lies heavily in favor of $W_2(O\text{-}i\text{-}Pr)_6$ such that the high-temperature limiting spectrum of the intramolecular dynamic process cannot be observed. However, even at +55 °C the septet b remains well resolved, and so equilibrium 1 is slow on the NMR time scale.

From these observations it is evident that four of the alkoxide ligands, namely those associated with the backbone tungsten atoms, are not involved in the fluxionality of the cluster. A preliminary line shape analysis of the ^{13}C signals associated with the methine carbons indicates that the energy of activation for the dynamic process is ca. 15 kcal mol^{-1}.[6] As noted before, a high-temperature limiting ^1H spectrum cannot be attained because

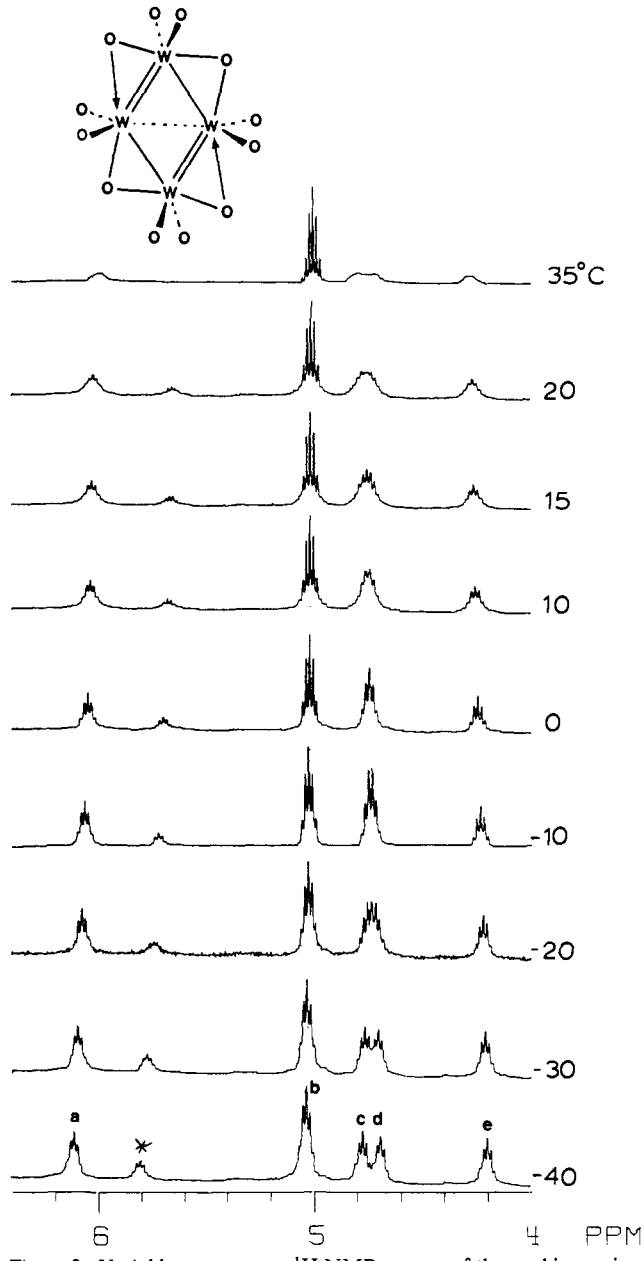

Figure 2. Variable-temperature ^1H NMR spectra of the methine region of $W_4(O\text{-}i\text{-}Pr)_{12}$. See text for explanation of labels: resonance * is due to $W_2(O\text{-}i\text{-}Pr)_6$.

the equilibrium lies heavily in favor of the dinuclear compound above 50 °C.

Inspection of the broadening of a, c, d, and e was suggestive of a pairwise and isoenergetic exchange process. 2D ^1H NMR chemical exchange experiments (NOESY) confirmed that exchange is occurring in a pairwise manner: a with d and c with e. See Figure 3. Selective bridge-terminal exchange cannot be operative or at least is not the threshold mechanism responsible for the observed NMR exchange. The latter would permute four different OR ligands: the two bridging OR groups and the two terminal OR groups on the wingtip tungsten atoms. It is also worthy of mention that added *i*-PrOH does not lead to line broadening of any of the cluster signals (a, b, c, d, e) though exchange with $W_2(O\text{-}i\text{-}Pr)_6$ is rapid leading to one time-averaged signal at room temperature. Moreover, the observations of the cluster dynamics are not concentration dependent.

The only plausible explanation that we can offer is the following. The cluster oscillates about a time-averaged symmetrical rhombus, i.e., through a D_{2h} $W_4(\mu\text{-}O)_4(O)_8$ transition state. This will lead to the equivalencing of the μ-OR ligands but will not exchange them with the terminal groups, i.e., the backbone and wingtip

(5) Maple, S. R.; Allerhand, A. *Anal. Chem.* **1987**, *55*, A441.
(6) Allerhand, A.; Maple, S. R.; Chisholm, M. H.; Hampden-Smith, M. J., work in progress.
(7) McQuarrie, D. A. *Statistical Mechanics*; Harper and Row Publishers: New York, 1976; pp 56 and 86.

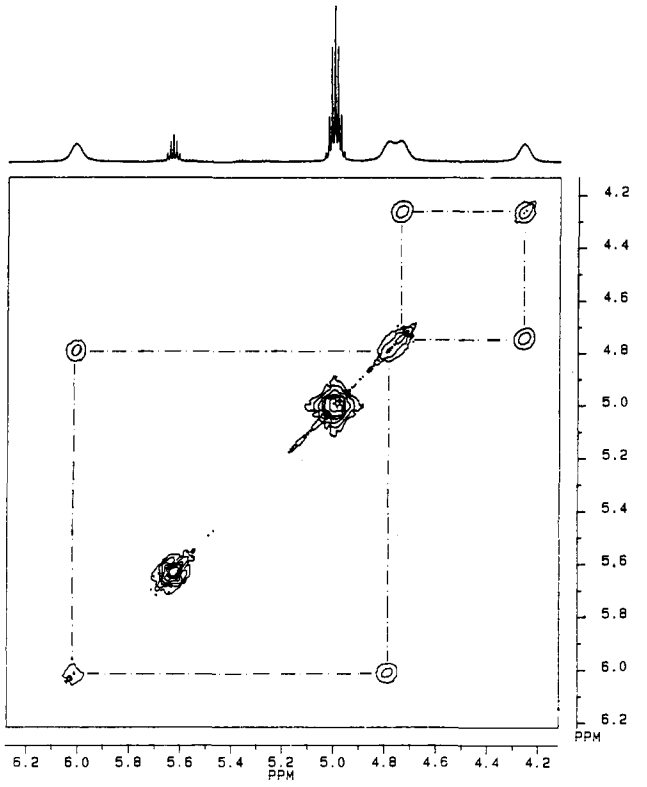

Figure 3. ^{1}H NMR 2D chemical exchange correlated countour plot of $W_4(O\text{-}i\text{-}Pr)_{12}$ at 26 °C (500.13 MHz) emphasizing the pairwise exchange between the methine protons. 2D matrix [1K (16 scans) × 256].

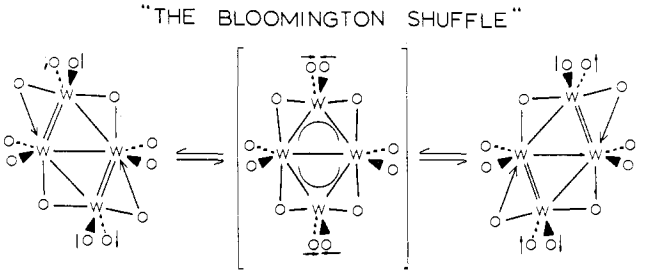

Figure 4. Schematic representation of the intramolecular dynamic exchange of the $W_4(\mu\text{-}O)_4(O)_8$ core of $W_4(O\text{-}i\text{-}Pr)_{12}$ together with methine vector reorientation about a time-averaged symmetrical (D_{2h}) rhomboidal framework of tungsten atoms.

W–O-*i*-Pr ligands will remain different. It is also necessary to invoke a correlated motion of the terminal wingtip W–OR groups such that the methine vectors are inverted. This combined motion we have named the *Bloomington Shuffle* and is diagramatically shown in Figure 4. The central $W_4(\mu\text{-}O)_4$ moiety moves little in this process as evidenced by the scale drawing shown in Figure 5 (scale 0.5 in. per Å as shown). The alternation of W=W and W—W bonds within the rhombus requires a 0.4-Å displacement of the wingtip tungsten atoms while the μ-O atoms pivot in a seesaw-like fashion moving only 0.5 Å. A square (D_{4h}) intermediate can be ruled out since this would make all terminal OR groups equivalent. The combined dynamics of the *Bloomington Shuffle* and equilibrium 1 provide for a metathesis of the tungsten atoms in the W–W triple bond, eq 2. Proof of metal atom scrambling must rest on a tungsten isotopic labeling experiment involving the use of tungsten compounds $W^*_2(O\text{-}i\text{-}Pr)_6$. Use of labeled alkoxide ligands is not a viable probe since (i) alkoxide group scrambling occurs within the cluster because of the formation of OR bridges and (ii) the coordinatively unsaturated $W_2(O\text{-}i\text{-}Pr)_6$ molecule exchanges O-*i*-Pr groups with free (fortuitous) *i*-PrOH. The latter would provide for a catalyzed scrambling of any labels associated with the alkoxide ligand.

$$W{\equiv}W + {}^*W{\equiv}{}^*W \rightleftharpoons W_2{}^*W_2 \rightleftharpoons 2{}^*W{\equiv}W \qquad (2)$$

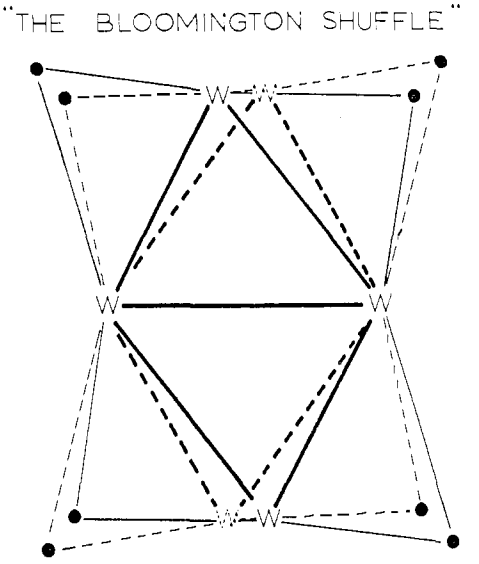

Figure 5. Scale drawing (0.5 in. per angstrom) of the limiting positions of the core $W_4(\mu\text{-}O)_4$ atoms of $W_4(O\text{-}i\text{-}Pr)_{12}$ in the *Bloomington Shuffle*.

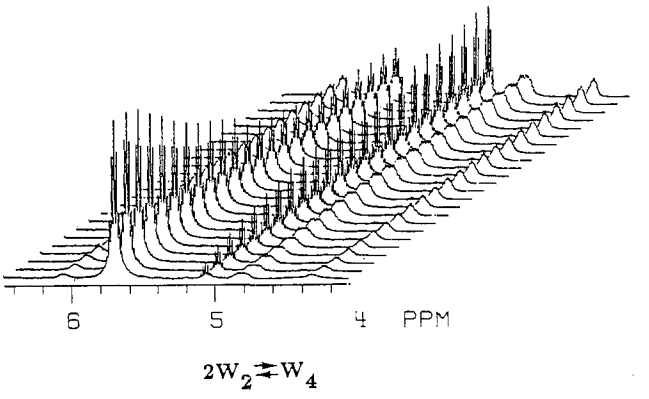

Figure 6. A stacked plot of ^{1}H NMR spectra (methine region) for a portion of one kinetic run of $2W_2(O\text{-}i\text{-}Pr)_6 \rightleftharpoons W_4(O\text{-}i\text{-}Pr)_{12}$ at 23 °C and 0.0277 M (in $W_4(O\text{-}i\text{-}Pr)_{12}$).

Studies of the Equilibrium between $W_4(O\text{-}i\text{-}Pr)_{12}$ and $W_2(O\text{-}i\text{-}Pr)_6$. Equilibrium constants for equilibrium reaction 1 have been measured over a temperature range 23 to 44 °C. Kinetic studies have been undertaken at room temperatures in the range +23 to +44 °C. Since the approach to equilibrium is laboriously slow below room temperature, and significant decomposition occurs above 50 °C, kinetic measurements were made directly on the dissociation of $W_4(O\text{-}i\text{-}Pr)_{12}$ and on the back reaction, the coupling of the two W≡W units within the temperature range noted above. Equilibrium constants were also measured at a different concentration. These three independent measurements reinforce confidence in the activation parameters derived from kinetic data measured over only a small temperature range. For the lower temperatures, the association or dissociation of eq 1 was followed for at least four half-lives, and at higher temperatures the approach to equilibrium was followed until equilibrium was established. Starting with either pure $W_2(O\text{-}i\text{-}Pr)_6$ or pure $W_4(O\text{-}i\text{-}Pr)_{12}$, each kinetic run was monitored by taking generally between 25 and 32 measurements of the relative conentrations of $W_4(O\text{-}i\text{-}Pr)_{12}$ and $W_2(O\text{-}i\text{-}Pr)_6$. The initial concentrations of either $W_4(O\text{-}i\text{-}Pr)_{12}$ or $W_2(O\text{-}i\text{-}Pr)_6$ were known, and the relative concentrations during the approach to equilibrium were determined by integrations of the methine resonance associated with $W_2(O\text{-}i\text{-}Pr)_6$ and that of the backbone O-*i*-Pr ligands of the cluster, namely resonance b in Figure 2. The latter represents one-third of the total integration of resonances for $W_4(O\text{-}i\text{-}Pr)_{12}$. A stacked plot for part of one typical kinetic run is shown in Figure 6.

A summary of the first-order rate constants, k_1, for the forward reaction, the second-order rate constants k_{-1} for the back reaction,

Table I. Summary of Rate Constants and Equilibrium Constants Together with the Thermodynamic and Activation Parameters for the Equilibrium $W_4(O\text{-}i\text{-}Pr)_{12} \rightleftharpoons 2W_2(O\text{-}i\text{-}Pr)_6$[h]

temp/°C	k_1[a]	k_{-1}[b]	K_{eq}[c]	K_{eq-1}[d]	K_{eq}*
44		7.2×10^{-3}	1.94×10^{-3}	58.67	
41				97.00	
38	4.7×10^{-5}	5.0×10^{-5}	8.31×10^{-3}	116.95	8.08×10^{-3}
35	1.8×10^{-5}	4.0×10^{-3}	5.48×10^{-3}	148.21	
34				177.39	
33				183.47	
32	1.7×10^{-5}	3.5×10^{-3}	4.28×10^{-3}	225.60	4.15×10^{-3}
28	1.1×10^{-5}	2.8×10^{-3}	2.28×10^{-3}	391.20	2.30×10^{-3}
26	6.0×10^{-6}	2.5×10^{-3}	2.04×10^{-3}	480.10	1.77×10^{-3}
23	2.7×10^{-6}	2.1×10^{-3}	1.61×10^{-3}	619.80	1.35×10^{-3}
free energies[e]	$\Delta G^{\ddagger}_{300} = +25$ (4)	$\Delta G^{\ddagger}_{300} = +22$ (2)	$\Delta G^{\circ}_{300} = +4$ (3)	$\Delta G^{\circ}_{300} = -3$ (2)	$\Delta G^{\circ}_{300} = +3$ (2)
enthalpies[e]	$\Delta H^{\ddagger} = +30$ (2)[g]	$\Delta H^{\ddagger} = +10$ (1)	$\Delta H^{\circ} = +22$ (2)	$\Delta H^{\circ} = -20$ (1)	$\Delta H^{\circ} = +22$ (1)
entropies[f]	$\Delta S^{\ddagger} = +18$ (6)	$\Delta S^{\ddagger} = -39$ (3)	$\Delta S^{\circ} = +61$ (6)	$\Delta S^{\circ} = -56$ (3)	$\Delta S^{\circ} = +62$ (3)

[a] s^{-1}. [b] mol^{-1} $L \cdot s^{-1}$. [c] mol L^{-1}. [d] mol^{-1} L. [e] kcal mol^{-1}. [f] cal K^{-1} mol^{-1} (eu). [g] Numbers in parentheses are estimated standard deviations. [h] Concentration of 0.0277 mol L^{-1} (in $W_4(O\text{-}i\text{-}Pr)_{12}$). K_{eq}* measurements were made at a concentration of 0.0653 mol L^{-1} (in $W_4(O\text{-}i\text{-}Pr)_{12}$). For a definition of terms see Experimental Section.

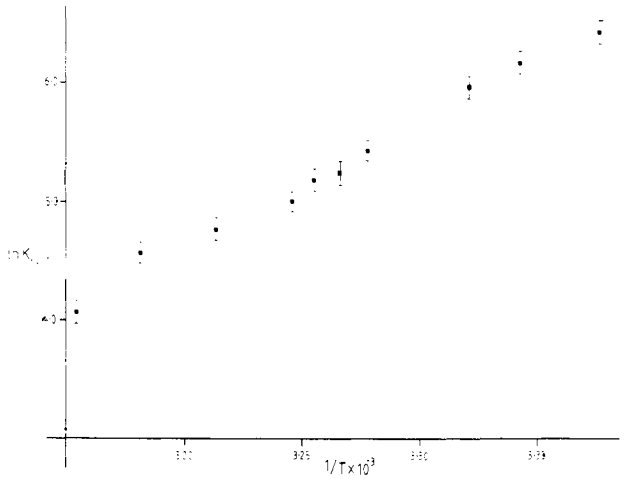

Figure 7. A plot of ln K_{eq}^{-1} vs $1/T$ to obtain the ground-state parameters for the association of $2W_2(O\text{-}i\text{-}Pr)_6$.

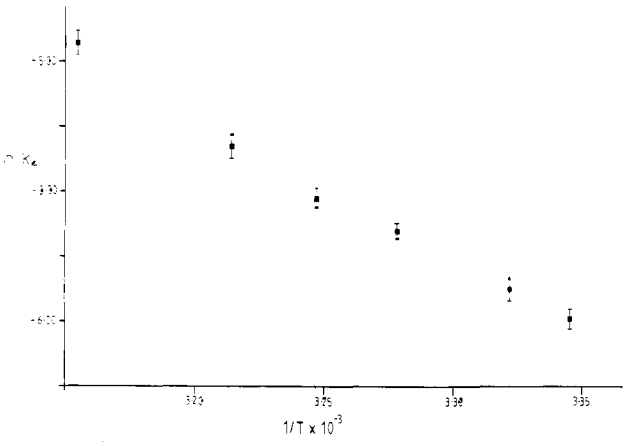

Figure 8. A plot of ln k_1 vs $1/T$ to obtain the activation parameters for the dissociation of $W_4(O\text{-}i\text{-}Pr)_{12}$.

and the equilibrium constants at different temperatures is given in Table I.

A plot of ln K_{eq}^{-1} versus $1/T$, Figure 7, gave the thermodynamic parameters for the reaction $2W_2 \rightarrow W_4$, $\Delta H^{\circ} = -21$ (1) kcal mol^{-1} and $\Delta S^{\circ} = -56$ (3) eu. Plots of log k_{-1} versus $1/T$ gave the activation parameters $\Delta H^{\ddagger} = +10$ (1) kcal mol^{-1} and $\Delta S^{\ddagger} = -39$ (3) eu for the coupling of two $W_2(O\text{-}i\text{-}Pr)_6$ units. A similar analysis for the forward reaction of eq 1 gave $\Delta H^{\ddagger} = +30$ (2) kcal mol^{-1} and $\Delta S^{\ddagger} = +18$ (6) eu. The thermodynamic and activation parameters are summarized in Table I. A plot of ln k_1 versus $1/T$ is shown in Figure 8.

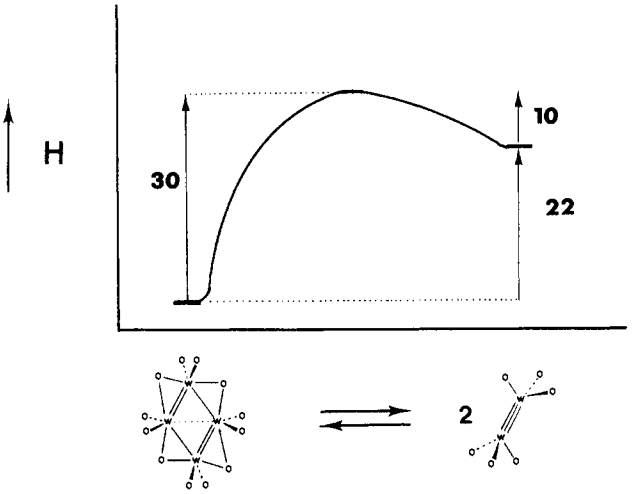

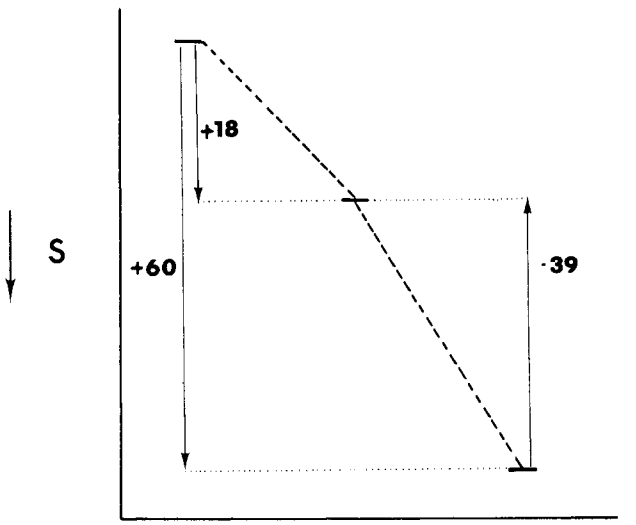

Figure 9. Schematic reaction coordinate for eq 1 separating enthalpy (A) and entropy (B) contributions to the free enthalpy of reaction. Enthalpy (kcal mol^{-1}) increases in the *upward* direction and entropy (entropy units) increases in the downward *direction*, such that both ΔH and ΔS are "uphill" in the upward direction.

These data combine to provide a comprehensive picture of the thermodynamic and kinetic aspects of the reversible coupling of the two $W_2(O\text{-}i\text{-}Pr)_6$ molecules. We can present the reaction profile in terms of an enthalpy and an entropy diagram, Figure 9.

The cluster is enthalpically favored but disfavored by entropy. The large difference in entropy of 61 eu undoubtedly has a significant contribution from a translational component due to the mass change 722 daltons versus 1444 daltons. The Sackur–Tetrode equation,[7] derived for a gas, predicts a difference in translational entropy of 44 eu. There are in addition entropy changes arising from restricted rotations in the cluster and from the differing solvation of the $W_2(O\text{-}i\text{-}Pr)_6$ and $W_4(O\text{-}i\text{-}Pr)_{12}$ molecules. Since $W_2(O\text{-}i\text{-}Pr)_6$ is a highly coordinatively unsaturated molecule, it is likely that it is well solvated and as a consequence the measured release in entropy ($\Delta S°$) on dissociation of $W_4(O\text{-}i\text{-}Pr)_{12}$ does not reflect the true entropy for formation of two free $W_2(O\text{-}i\text{-}Pr)_6$ molecules (as it might be in the gas phase, for example). This effect has recently been demonstrated dramatically for the dimer–tetramer equilibrium shown in eq 3.[8]

$$[LiC{\equiv}C\text{-}t\text{-}Bu]_4 \rightleftharpoons 2[LiC{\equiv}C\text{-}t\text{-}Bu]_2 \qquad (3)$$

In 3 $\Delta S°$ for dissociation is *ca.* −40 eu due to the higher solvation of the dimeric species. A similar situation is common for solvolysis (S_N1) of alkyl halides in polar solvents.[9] The solvation of $W_2(O\text{-}i\text{-}Pr)_6$ by toluene molecules it not unreasonable in view of the recent preparation of $W_2(OCH_2\text{-}t\text{-}Bu)_6(\eta^2\text{-}C_2H_4)_2$ and the observation that it exists in the reversible equilibrium shown below, eq 4.[10] In benzene solution, equilibrium 4 lies well to the left

$$W_2(OCH_2\text{-}t\text{-}Bu)_6(\eta^2\text{-}C_2H_4)_2 \rightleftharpoons W_2(OCH_2\text{-}t\text{-}Bu)_6 + 2C_2H_4 \qquad (4)$$

at room temperature. $W_2(O\text{-}i\text{-}Pr)_6$ also reacts with ethylene at room temperature to form a compound of formula $W_2(O\text{-}i\text{-}Pr)_6(CH_2)_4(C_2H_4)$ in which two ethylene molecules have been coupled to form a metallacyclopentane and a third is present as a $\eta^2\text{-}C_2H_4$ ligand.[11] Clearly some weak toluene solvation of $W_2(O\text{-}i\text{-}Pr)_6$ seems likely.

From the activation parameters, it appears that the transition state resembles the cluster but with slightly less order. It also appears that on forming the $W_4(O\text{-}i\text{-}Pr)_{12}$ cluster from two $W_2(O\text{-}i\text{-}Pr)_6$ molecules, the small enthalpy of activation indicates that no strong bonds are broken. Conversely, on dissociation of $W_4(O\text{-}i\text{-}Pr)_{12}$, bonds are broken to reach the transition state ($\Delta H^‡$ = +30 kcal mol^{-1}).

It is thus not unreasonable to suppose that alkoxide bridge formation and rupture represents the rate-determining step for cluster formation and dissociation, respectively. The enthalpy of activation is positive in both directions. As the cluster is pulled apart there will be a loss of metal–metal cluster bonding while for the coupling formation of alkoxide bridges is almost enthalpically neutral, but a small positive enthalpy of activation can be understood in terms of a loss of alkoxide-to-tungsten π-bonding, and a reorganization of the remaining W–OR bonds. At this point is it worth mentioning that the tetranuclear compound $Mo_4(\mu\text{-}F)_2(\mu\text{-}O\text{-}i\text{-}Pr)_2(O\text{-}i\text{-}Pr)_8$ has been structurally characterized and is known to be formed reversibly even at temperatures below −20 °C.[12] Here there is a Mo_4 rectangle involving two localized Mo≡Mo bonds, 2.24 Å, and two Mo-to-Mo nonbonding distances, 3.5 Å. More recently we have observed that the reaction between $Mo_2(O\text{-}i\text{-}Pr)_6$ and 1 equiv of methanol results in formation of $Mo_4(\mu\text{-}OMe)_2(\mu\text{-}O\text{-}i\text{-}Pr)_2(O\text{-}i\text{-}Pr)_8$ in which two Mo≡Mo triple bonds are united by alkoxide bridges.[13] The importance of alkoxide bridge formation on association of two $W_2(O\text{-}i\text{-}Pr)_6$ molecules is also borne out by the observation that *none* of $W_2(OR)_6$, where R = *t*-Bu, adamantyl, 1-adamantylmethyl, and cyclohexyl, undergo cluster formation in toluene solution while $W_2(OCH_2\text{-}t\text{-}Bu)_6$ and $W_2(O\text{-}c\text{-}C_5H_9)_6$ do form cluster compounds under identical conditions but much more slowly than $W_2(O\text{-}i\text{-}Pr)_6$ and irreversibly.[14] The apparent importance of steric accessibility of the alkoxide oxygen atom in the cluster-forming process is entirely consistent with steric parameters derived from rates of acid-catalyzed esterification of carboxylic acids.[15] These results are also consistent with studies of the oligomerization of alkyl tin(IV) alkoxides, $(R_{4-x})Sn(OR')_x$, using ^{119}Sn NMR spectroscopy and molecular weight determinations.[16] It was demonstrated that the enthalpic driving force for oligomerization (i.e., the formation of bridging alkoxide ligands) was offset by a high entropic barrier. With sufficiently sterically demanding alkoxide ligands (or inaccessible oxygen atoms), e.g., where R' = *tert*-Bu, association was completely inhibited.

Table II. Selected Entropies of Activation for Diels–Alder Cycloaddition Reactions (from Ref 17)

diene	dienophile	$\Delta S^‡$, eu
cyclopentadiene	cyclopentadiene	−38 to −28[a]
cyclopentadiene	17 dienophiles	−38 to −29
anthracene	tetracyanoethylene	−49 to −30[a]
7 dienes	maleic anhydride	−42 to −33

[a] Data recorded in different solvents.

Clearly in the coupling of two $W_2(O\text{-}i\text{-}Pr)_6$ units the initial W-μ-OR-W bond formation could occur without inducing any W–W cluster bonding. Nevertheless the large magnitude of $\Delta S^‡$ = −39 eu for the coupling of the two $W_2(O\text{-}i\text{-}Pr)_6$ units suggests a highly ordered transition state and indeed is reminiscent of many cycloaddition reactions in organic chemistry. See Table II. While the coupling of two C≡C bonds to give cyclobutadiene or two P≡P bonds to give tetrahedral P_4 is known to be a symmetry-forbidden reaction,[18-20] we were intrigued at the prospect that the coupling of two W≡W units to give the rhomboidal $W_4(O\text{-}i\text{-}Pr)_{12}$ molecule might be a symmetry-allowed reaction. Accordingly, we investigated this possibility with the aid of MO calculations.

A Symmetry-Allowed $[\pi^2_s + \pi^2_s]$ Cycloaddition Reaction? The organic counterpart, the concerted $[\pi^2_s + \pi^2_s]$ cycloaddition of two acetylene molecules to yield cyclobutadiene, is a forbidden reaction in the Woodward–Hoffmann sense.[18-20] The presence of metal d functions will complicate the simple Woodward–Hoffmann picture, but it would be naive to assume that the presence of d orbitals would automatically make such a process allowed. The idea of a possible concerted suprafacial cycloaddition of two $M_2(OR)_6$ (M≡M) compounds occurred to us while we were investigating the effect of the second-order Jahn–Teller distortion on the symmetrical D_{2h} rhombus.[1]

Before discussing possible mechanisms, it is useful to first consider a heuristic discussion comparing the cycloaddition of two acetylene molecules with the cycloaddition of two $M_2(OR)_6$ molecules. During the suprafacial dimerization of two acetylene molecules, a very large symmetry-imposed barrier arises because two ground-state acetylene molecules correlate with a very high energy excited state of cyclobutadiene. This statement is not necessarily true when considering the suprafacial dimerization of two $M_2(OR)_6$ molecules, since the presence of d orbitals adds "flexibility" to the system such that they may combine in a trapezoidal fashion. If a trapezoidal (or rhomboidal) approach is employed for the reaction, then there is an additional overlap between basis orbitals across the diagonal (or backbone) which will be stabilizing.

(8) Sprague, B.; Fraenkel, G.; Chow, A. 18th Central Regional ACS Meeting, 1987, Abstract No. 301.
(9) March, J. *Advanced Organic Chemistry*, 3rd ed.; Wiley Publishers: New York, 1985; pp 259–260.
(10) Chisholm, M. H.; Hampden-Smith, M. J. *Angew. Chem., Int. Ed. Engl.* **1987**, *26*, 903.
(11) Chisholm, M. H.; Hampden-Smith, M. J. *J. Am. Chem. Soc.*, submitted; *J. Am. Chem. Soc.* **1987**, *109*, 5871.
(12) Chisholm, M. H.; Clark, D. L.; Errington, R. J.; Huffman, J. C. *Inorg. Chem.* **1988**, *27*, 2701.
(13) Chisholm, M. H.; Hammond, C. E.; Hampden-Smith, M. J.; Huffman, J. C.; Van Der Sluys, W. G. *Angew. Chem., Intl. Ed. Engl.* **1987**, *26*, 904.
(14) Chisholm, M. H.; Hampden-Smith, M. J., results to be published.
(15) Charton, M. *J. Am. Chem. Soc.* **1975**, *97*, 1552.
(16) Kennedy, J. D. *J. Chem. Soc., Perkin Trans. II* **1977**, 242.
(17) Taken from: *Angew. Chem., Intl. Ed. Engl.* **1980**, *19*, 779.
(18) Woodward, R. B.; Hoffmann, R. *The Conservation of Orbital Symmetry*; Academic Press: New York, 1969.
(19) Salem, L. *Electrons in Chemical Reactions*; Wiley: New York, 1982.
(20) Albright, T. A.; Burdett, J. K.; Wangbo, M. H. *Orbital Interactions in Chemistry*; Wiley: New York, 1985.

Since it does not matter from which point of the reaction one starts, let us consider the hypothetical concerted cycloreversion of $W_4(OR)_{12}$ to yield two molecules of $W_2(OR)_6$. We begin with a symmetrical D_{2h} rhombus and distort along the b_{1g} vibrational coordinate until the rhombus decomposes into two $W_2(OR)_6$ fragments as illustrated in eq 5 below. Note that the $M_2(OR)_6$ fragments generated in this fashion only differ little from the idealized staggered "ethane-like" geometry of $W_2(OR)_6$ as illustrated in eq 5 below. We have examined the possible cycloreversion process using the Fenske–Hall method[21] with the full details specified in the section on computational procedures. The origin for this concerted cycloreversion process was chosen to be the Jahn–Teller distorted C_{2h} rhombus which we discussed in detail in the previous paper.[1] In order to make the reaction coordinate

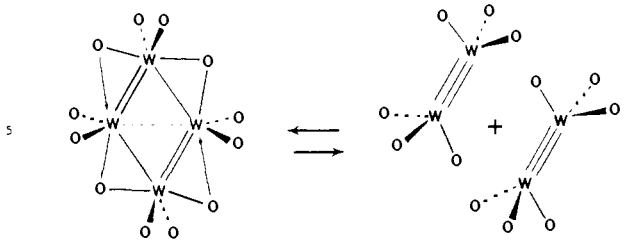

(5)

more tractable, the "short" W–W distance of 2.50 Å was held constant as were the W–O distances and W–O–H angles. Our justification for this simplification came from two calculations on idealized $W_2(OH)_6$ models with W–W distances of 2.315 and 2.502 Å. This confirmed the intuitive result that, as far as orbital symmetry is considered, a triple bond at a distance of 2.3 or 2.5 Å looks the same. The actual reaction coordinate consists of 10 synchronous regular variations of (i) bond angles and (ii) the "long" W–W distances (in a trapezoidal manner) while maintaining C_{2h} symmetry.

Is this simple C_{2h} cycloreversion $W_4(OR)_{12} = 2W_2(OR)_6$ a symmetry-allowed process? On the $W_4(OR)_{12}$ side of the reaction coordinate, the four W–W σ bonds transform as $2a_g + 2b_u$, and the two W–W π bonds transform as $a_u + b_g$. On the $W_2(OR)_6$ side the set of W–W σ bonds and W–W π bonds contained in the W_4-plane transform as $2a_g + 2b_u$, and the set of W–W π bonds perpendicular to the W_4-plane transform as $a_u + b_g$. The reaction appears to have the components of a symmetry-allowed reaction in the C_{2h} point group.[22]

Tracing the Cycloreversion Process. A Walsh diagram for the concerted cycloreversion of $W_4(OH)_{12}$ to two $W_2(OH)_6$ molecules under C_{2h} symmetry is displayed in Figure 10. There are no real level crossings between occupied and unoccupied molecular orbitals of the reactant and products and thus the dimerization process is allowed in the Woodward–Hoffmann sense under C_{2h} symmetry. On the left side of the Walsh diagram in Figure 10 are the important primarily metal–metal bonding and antibonding molecular orbitals of C_{2h} $W_4(\mu\text{-}OH)_4(OH)_8$, and on the right are those of two molecules of $W_2(OH)_6$ at a 2.502 Å W–W distance. The HOMO of both reactant and product are denoted by arrows. From the Walsh diagram we can see that the dimerization of two $W_2(OH)_6$ molecules results in a stabilization of all the occupied metal–metal bonding combinations. So it is clear why two $W_2(OR)_6$ molecules are enthalpically unstable with respect to oligomerization to form a $W_4(OR)_{12}$ cluster when the steric bulk of R is sufficiently reduced as in the case of the isopropoxide ligands. Conversely, the height of the electronic hill that $W_4(OH)_{12}$ orbitals must climb in order to dissociate into two molecules of $W_2(OH)_6$ is not very high relative to that which would have to be surmounted by the organic counterpart, cyclobutadiene. Thus it is not hard to see why at +65 °C, in hydrocarbon solvents, $W_4(O\text{-}i\text{-}Pr)_{12}$ is essentially completely dissociated into two molecules of $W_2(O\text{-}i\text{-}Pr)_6$ as determined by ^1H NMR studies. In this regard we note that another well-known reversible dimerization

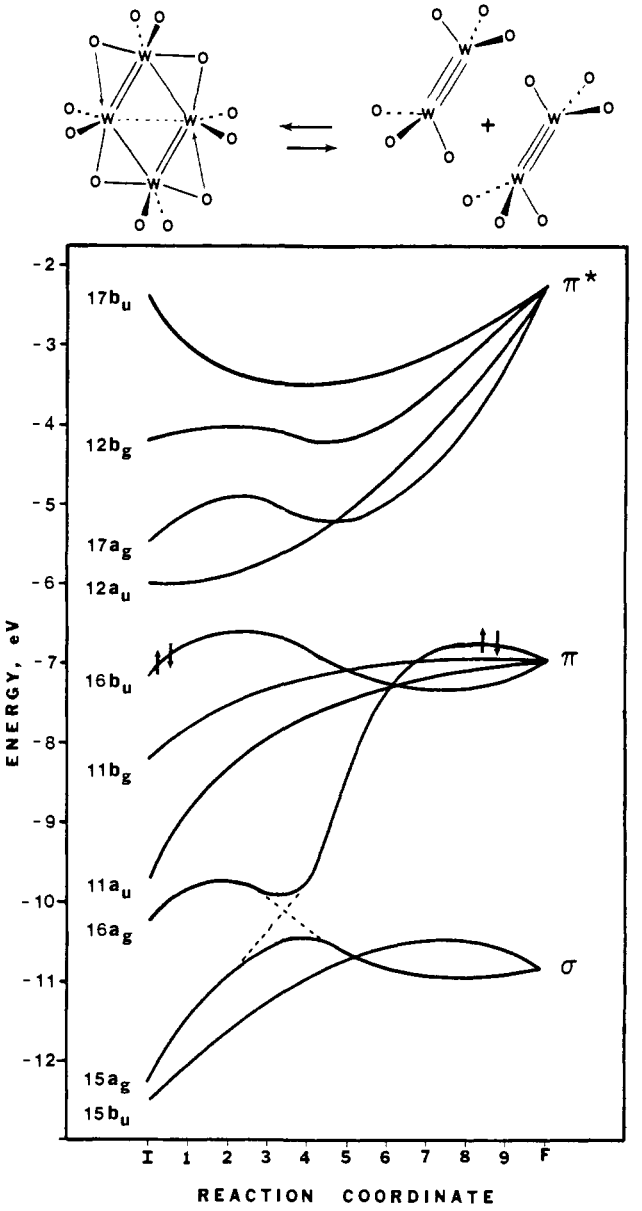

Figure 10. A Walsh diagram for the concerted $[\pi^2_s + \pi^2_s]$ cycloreversion process. The predominantly metal-based orbitals of the Jahn–Teller distorted C_{2h} $W_4(\mu\text{-}OH)_4(OH)_8$ molecule are shown at left, and those of two molecules of $W_2(OH)_6$ are shown at right.

of inorganic $\sigma^2\pi^4$ triple bonds is that of the $P_2 \rightleftarrows P_4$ equilibrium observed at 1100 K.[23] It has been shown that the concerted D_{2d} dimerization of P_2 to yield T_d P_4 is a symmetry-forbidden reaction, just as is the coupling of two ethyne molecules to give tetrahedrane along the same reaction coordinate.[23] The reasoning behind the "symmetry-forbiddenness" of this reaction is that two ground-state P_2 molecules (or C_2H_2 molecules) must correlate with an excited-state P_4 molecule (or tetrahedrane) thereby generating a tremendous electronic hill that must be surmounted by the P_2 molecules upon dimerization. Thus at room temperature, the P_4 molecule is stable with respect to cycloreversion to generate P_2. However, at temperatures in excess of 1100 K, where we are surely dealing with an excited-state P_4 molecule, the equilibrium is observed and is driven toward P_2 by entropy.[24]

Let us now take a more detailed look at the actual transformation of $W_4(OH)_{12}$ into two molecules of $W_2(OH)_6$. The transformation of the $11b_g$ and $11a_u$ π-bonding orbitals of W_4-

(21) Hall, M. B.; Fenske, R. F. *Inorg. Chem.* **1972**, *11*, 768.
(22) This is essentially an application of the orbital symmetry rules suggested by Pearson. Pearson, R. G. *J. Am. Chem. Soc.* **1972**, *29*, 8287.
(23) For an excellent discussion see: Bock, H.; Muller, H. *Inorg. Chem.* **1984**, *23*, 4365 and references therein.
(24) For the reaction $P_4 \rightleftarrows 2P_2$, $\Delta H° = +55.5$ kcal mol^{-1} and $\Delta S° = +25.6$ eu. From ref 23.

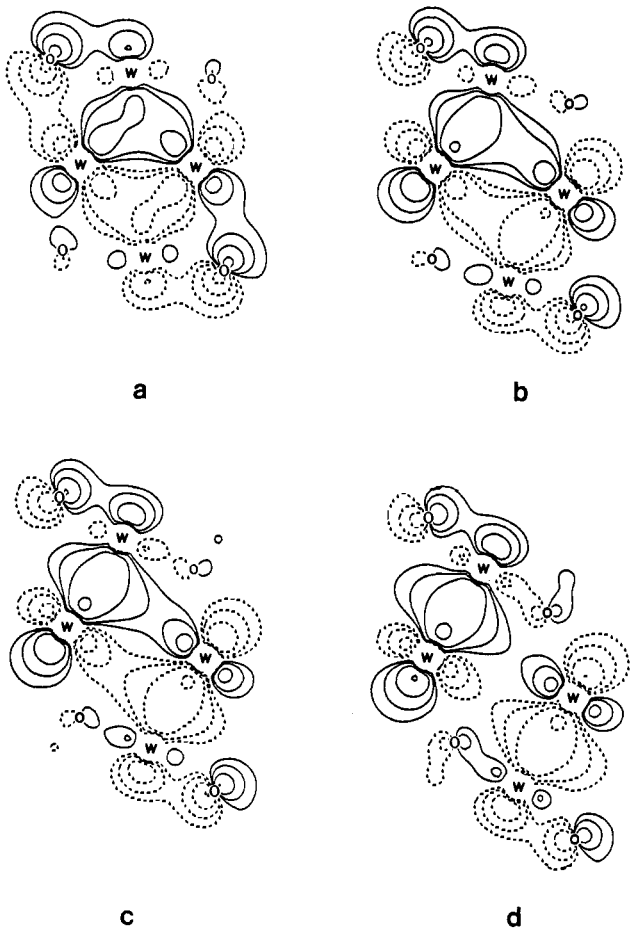

Figure 11. Contour plots following the transformation of the $15b_u$ orbital of $W_4(\mu\text{-}OH)_4(OH)_8$ into the b_u combination of two σ-bonding orbitals of $W_2(OH)_6$ when viewed in the sequence a, b, c, and d.

Table III. Percent Contribution from C_2^{2-} Fragment Orbitals in Relevant Molecular Orbitals of C_4H_4 at Selected Points Along the C_{2h} Reaction Coordinate (I = initial; F = final)

	$4b_u$						$5b_u$					
	I	2	4	6	8	F	I	2	4	6	8	F
$1\sigma_g$	0	1	0	0	0	0	17	10	5	2	0	0
$1\sigma_u$	4	6	5	0	0	0	0	0	1	2	0	0
$1\pi_u$	0	1	10	65	94	100	74	83	81	31	5	0
$2\sigma_g$	0	1	1	2	0	0	9	6	3	0	0	0
$1\pi_g$	74	77	76	30	5	0	0	1	9	63	94	100
$2\sigma_u$	1	0	0	0	0	0	0	0	0	0	0	0

$(OH)_{12}$ into sets of π-bonding orbitals of two $W_2(OH)_6$ molecules is straightforward and easily visualized. These transformations are illustrated qualitatively in I. In a similar fashion, the $15b_u$

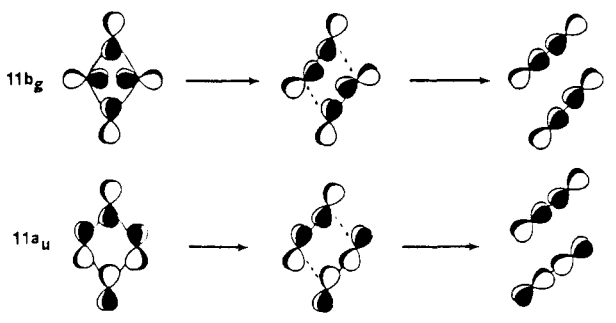

I

and $16b_u$ orbitals of $W_4(OH)_{12}$ correlate with the set of $W_2(OH)_6$ σ- and π-bonding combinations, respectively. Depiction of these transformations via qualitative drawings is admittedly much more difficult. Therefore, it was decided to illustrate these transformations both qualitatively, as shown in II, and more quantitatively

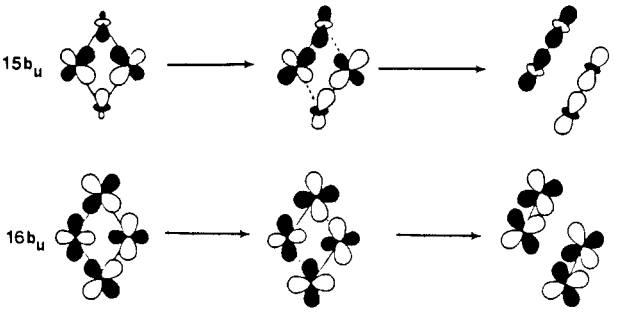

II

with the aid of contour plots taken at various stages along the reaction coordinate. These plots are very instructive and are shown for the $15b_u$ and $16b_u$ transformations in Figures 11 and 12, respectively. Finally we illustrate the transformation of $15a_g$ and $16a_g$ orbitals of $W_4(OH)_{12}$ into the respective σ and π combinations of two $W_2(OH)_6$ molecules. A simplified orbital correspondence based on orbital composition, and without taking into account the avoided crossings, is shown for the metal-based a_g orbitals in Figure 13a. The $15a_g$ orbital of $W_4(OH)_{12}$ corresponds to the a_g π-bonding combination on the $W_2(OH)_6$ side of the reaction coordinate. In a similar fashion, the $16a_g$ orbital of $W_4(OH)_{12}$ corresponds with the a_g σ-bonding combination on the $W_2(OH)_6$ side of the reaction coordinate. Now, taking into account the necessary avoidance of orbitals of the same symmetry, the approximate correlations of Figure 13b take place. The $15a_g$ orbital correlates with the a_g σ-bonding combination of two $W_2(OH)_6$ molecules, and the $16a_g$ orbital of $W_4(OH)_{12}$ correlates with the a_g π-bonding combination of two $W_2(OH)_6$ molecules. This avoided crossing is denoted in the Walsh diagram of Figure 10 with dashed lines. In reality other avoided crossings occur because there are other orbitals of the same symmetry, but the fundamental transformation is depicted here in simplified form. Furthermore, it should be noted that this avoided crossing is of no consequence to the "allowedness" of the reaction. The avoided crossing between $16a_g$ and $15a_g$ orbitals is only weakly avoided and was found to be very dependent on the W–W–O angle. It is instructive to follow the rehybridization that takes place near the avoided crossing, and accordingly, contour plots that trace the $15a_g$ and $16a_g$ orbitals through the avoided crossings are shown in Figures 14 and 15, respectively.

Probing the Memory of Symmetry-Allowed and Symmetry-Forbidden Pathways in Lower Symmetry Groups. It might happen that a bonding–antibonding avoided crossing has gone undetected due to the complexity and low symmetry of the system, and that the *intended* correlations remain. For organic systems, large energy barriers appear as the remnants of the intended but avoided crossing and reflect the inherent forbiddenness of the reaction.[16-18] During the course of this study it was suggested that such an inherent barrier to the $2\pi + 2\pi$ symmetry-forbidden reaction may still be present.[25] In response to this criticism, a series of experiments/calculations were performed that we feel demonstrate the "allowedness" of this reaction in a simple, readily understandable manner. Moreover, the process may be equally applied to inorganic or organic systems.

In order to establish the credibility of the experiment, we first show that this method will work on a well-known example. We generate a Walsh diagram for the interconversion of $2C_2H_2$ to C_4H_4 along a C_{2h} pathway in parallel with that done for $W_4(OH)_{12}$. This pathway is illustrated schematically in III. A Walsh diagram for this mechanism was constructed with the Fenske–Hall method, beginning with rectangular C_4H_4 and C–C distances of 1.35 and 1.50 Å for the double and single bonds, respectively. The H–C–C angle was varied from an initial 135° to a final 180°. As in the $W_4(OH)_{12}$ calculation, this was accomplished in 10

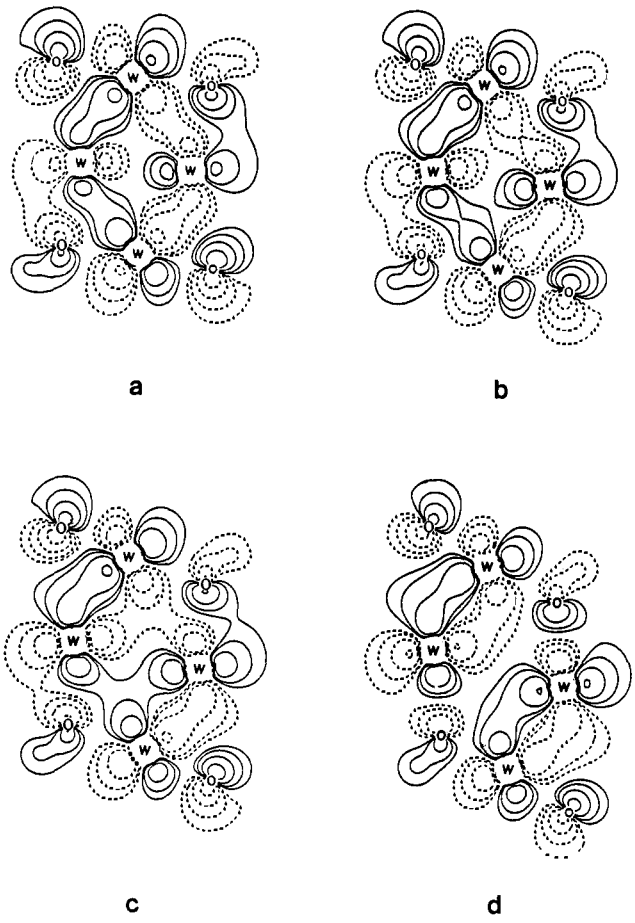

Figure 12. Contour plots following the transformation of the $16b_u$ orbital of $W_4(\mu\text{-}OH)_4(OH)_8$ into the b_u combination of two π-bonding orbitals of $W_2(OH)_6$ when viewed in the sequence a, b, c, and d.

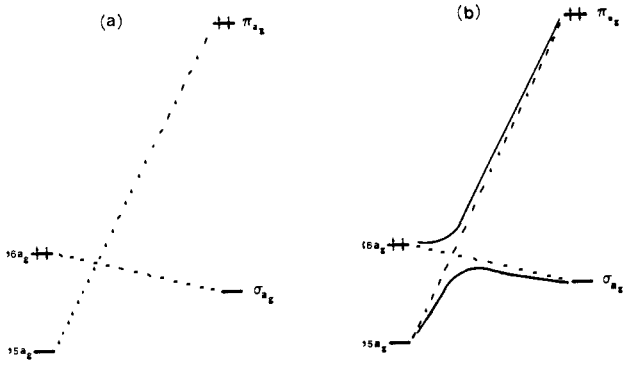

Figure 13. The correlation of the $15a_g$ and $16a_g$ orbitals of $W_4(\mu\text{-}OH)_4(OH)_8$ with the a_g combinations of σ and π orbitals of $W_2(OH)_6$ (a) before taking into account avoided crossings and (b) after taking into account avoided crossings.

synchronous regular variations in H–C–C angle and "long" C–C distance while maintaining a "short" C–C distance of 1.35 Å throughout. Since the result is well-known, it is simply summarized here qualitatively in III for the important $4b_u$ and $5b_u$ orbitals. Even though we have reduced the symmetry by using a trapezoidal reaction coordinate, a bonding level of reactants has still moved to high energy in the transition state. The Fenske–Hall method calculates an energy barrier of ca. 8 eV which appears as the remnant of the intended bonding–antibonding correlation. In order to demonstrate this inherent forbiddenness to an unbelieving observer, we must find some way to probe the "memory" of this system to see if it "remembers" that it is indeed a forbidden reaction. To achieve this, three more calculations were performed

(25) Hoffmann, R., personal communication.

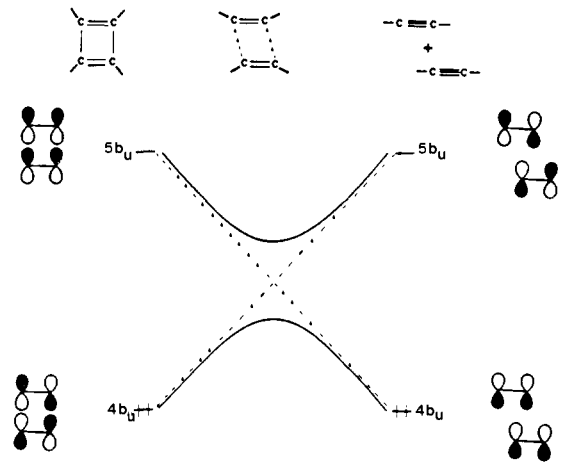

III

for each point in the Walsh diagram. Two separate calculations were performed on two "naked" diatomics, C_2^{2-}, with the same C–C distances, 1.35 Å, and same position in space as in our model C_4H_4. Next, the vectors of C_2^{2-} are assigned to the appropriate symmetry labels which yield the expected (ignoring the 1s) $1\sigma_g$, $1\sigma_u$, $1\pi_u$, $2\sigma_g$, $1\pi_g$, and $2\sigma_u$ orbitals. These orbitals are sketched qualitatively in IV. Finally, the converged vectors of C_4H_4 were

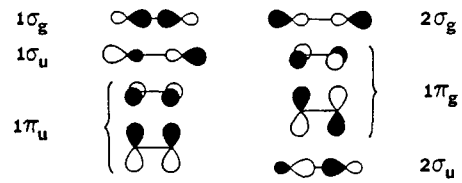

IV

transformed into a basis consisting of the canonical orbitals of our two separate C_2^{2-} fragments at the identical C–C distance and positions. The results of this basis transformation for the important $4b_u$ and $5b_u$ orbitals are given in Table III and are really quite revealing. Note that the occupied $4b_u$ orbital of C_4H_4 in the initial rectangular geometry (point I) is composed of 74% of the $1\pi_g$ (π^*) orbitals of two C_2^{2-} moieties. That is to say that the $4b_u$ orbital "remembers" that it was originally a π^* orbital in the two separated C_2^{2-} entities. As we follow the $4b_u$ orbital along the reaction coordinate we see that it mixes with the $1\pi_u$ (π) orbital and ends up as 100% of the $1\pi_u$ orbital in separated C_2H_2 molecules (point F). This illustrates that the C_2^{2-} fragments act as a convenient probe into the memory of the forbiddenness of the interconversion of C_2H_2 to C_4H_4. Notice also that at point 6 of the reaction coordinate (Table III) the $4b_u$ orbital is an admixture of both the $1\pi_u$ and $1\pi_g$ orbitals as expected from considerations of simple perturbation theory near the avoided crossing. A similar phenomenon can be seen in the unoccupied $5b_u$ orbital. It starts out in C_4H_4 as predominantly $1\pi_u$ (point I) and ends up as 100% $1\pi_g$ in the separated acetylene molecules (point F). The important message from this experiment is that even though the crossing is avoided because of reduced symmetry, our probe clearly reveals that this reaction is forbidden and a clear memory of the event is contained in the percent characters of the transformed basis. The intent of these orbitals to cross as well as the inherent barrier to dimerization is still present, and as such it is a real crossing, only trivially avoided. The other important observation is that the $4b_u$ (π) orbital of C_2H_2 must rise very high in energy (ca. 8 eV, as calculated by the Fenske–Hall method) in order to get from reactant to products. This is obviously nothing new, but it is important to show that the memory of the reaction can be probed by such a basis transformation. Now that we have this precedent, we apply this technique to the $W_2(OR)_6$ dimerization.

In order to probe the memory of the interconversion of $W_2(OR)_6$ to $W_4(OR)_{12}$ we will employ the set of canonical orbitals

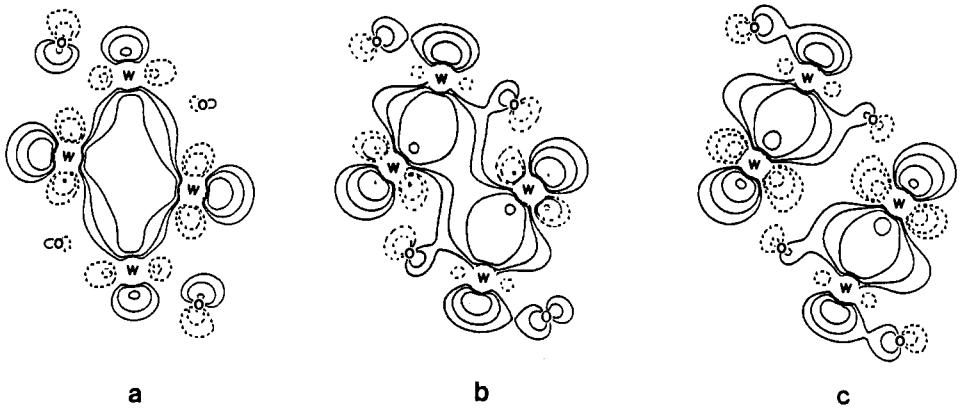

Figure 14. Contour plots following the transformation of the $15a_g$ orbital of $W_4(\mu\text{-}OH)_4(OH)_8$ into the a_g combination of two σ-bonding orbitals of $W_2(OH)_6$.

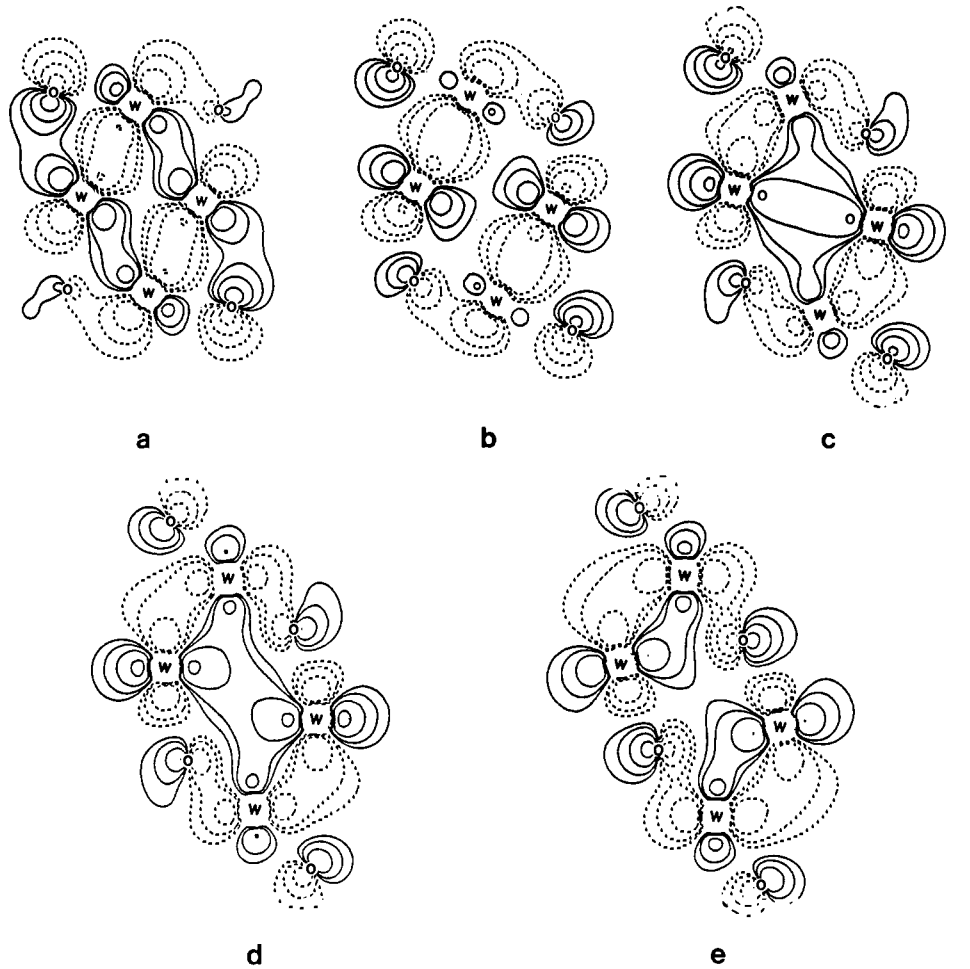

Figure 15. Contour plots following the transformation of the $16a_g$ orbital of $W_4(\mu\text{-}OH)_4(OH)_8$ into the a_g combination of two π-bonding orbitals of $W_2(OH)_6$.

Table IV. Percent Contribution from W_2^{6+} Fragment Orbitals in Relevant Molecular Orbitals of D_{3d} $W_2(OH)_6$

	$4a_{1g}$	$5e_u$	$5e_g$	$4a_{2u}$
σ_g	75	0	0	0
π_u	0	66	0	0
δ_g	0	0	45	0
δ_u	0	1	0	0
π_g	0	0	33	0
σ_u	0	0	0	75
6_s	19	0	0	0
6_p	0	4	0	16

of two W_2^{6+} fragments. This is a bit more complicated than the C_2^{2-} transformation because the M–M π and π^* orbitals are not composed of simply π_u and π_g orbitals but rather are a mixture of M–M π and δ character. A calculation of W_2^{6+} at a W–W distance of 2.50 Å yields the expected σ_g, π_u, δ_g, δ_u, π_g, and σ_u M–M components of a naked metal diatomic as illustrated qualitatively in V. Let us examine a simple $W_2(OH)_6$ model compound under D_{3d} symmetry with W–W = 2.50 Å to be sure we understand it first. The important orbitals in the metal–metal bonding manifold are the $4a_{1g}$ (σ), $5e_u$ (π), $5e_g$ (π^*), and $4a_{2u}$ (σ^*) orbitals. The percent contribution from W_2^{6+} fragment orbitals to these $W_2(OH)_6$ orbitals are listed in Table IV. The important observation here is that the metal–metal π orbital ($5e_u$) is predominantly the π_u orbital of W_2^{6+} with a mere 1% metal–metal δ_u contribution (a result that mimics the PXα calculation reported by Cotton et al. on $Mo_2(OH)_6$).[26] By contrast, the metal–metal

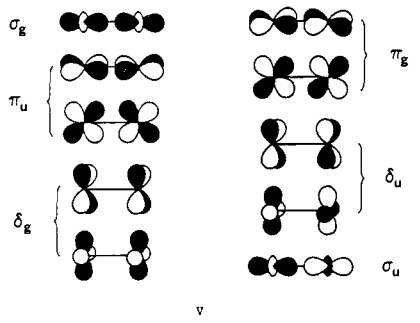

V

π^* orbital ($5e_g$) is an admixture of W_2^{6+} δ_g and π_g character. To help illustrate this mixing, contour plots of the π ($5e_u$) and π^* ($5e_g$) orbitals of our $W_2(OH)_6$ model are shown in Figure 16. The δ_g mixing in the π^* orbital is very apparent in the plot and it effectively minimizes the metal–metal antibonding in the π^* orbital. We feel that this mixing is real and actually manifests itself in the extremely low intensity of the $\pi \rightarrow \pi^*$ transition (ϵ = 2000 M^{-1} cm^{-1}) in these molecules[27] for the same reason that the well-known $\delta \rightarrow \delta^*$ transition in quadruple bonds is inherently weak.[28]

The Walsh diagram for the interconversion of $W_2(OH)_6$ to $W_4(OH)_{12}$ was shown in Figure 10. Recall that there is an avoided crossing that occurs between the occupied $15a_g$ and $16a_g$ orbitals, although this is of no consequence to the "allowedness" of the reaction. Let us see whether or not we can use the canonical orbitals of two W_2^{6+} fragments to probe the memory of this avoided crossing. Shown in the top portion of Table V are the percent contributions from W_2^{6+} fragment orbitals in the $15a_g$ and $16a_g$ orbitals of $W_4(OH)_{12}$ at selected points along the C_{2h} reaction coordinate. Notice that the $15a_g$ orbital starts out as a mixture of predominantly π_u and 6s character (point I). Proceeding along the reaction coordinate, a mixing of π_u and σ_g character is evident as the orbital is converted into the σ orbitals of separated $W_2(OH)_6$ fragments (point F). This σ_g–π_u mixing is most pronounced at point 4, which, from the Walsh diagram, is about the point where the avoided crossing takes place. For the $16a_g$ orbital a similar trend can be seen. It starts out (point I) as predominantly the σ_g orbital, mixes with the π_g orbital near the avoided crossing, and transforms into the π_u orbital of separated $W_2(OH)_6$ entities. Thus our probe reveals that this is an avoided crossing since a complete memory of the event is contained in the percent W_2^{6+} characters.

The above discussion is intended to establish that a basis transformation is a reliable tool for probing the memory of an avoided crossing. Through the basis transformation, the intent of two orbitals to cross is clearly revealed in the percent characters of the transformed basis. The technique works for the organic system and reveals that a C_{2h} pathway for C_2H_2 dimerization is a forbidden reaction. It also works for the inorganic system and has revealed the avoided a_g crossing in the $W_2(OH)_6$ dimerization under C_{2h} symmetry as well.

The all important question concerning the $W_2(OR)_6$ dimerization is whether or not there exists an avoided crossing between the occupied $16b_u$ and unoccupied $17b_u$ orbitals in parallel to that seen in C_4H_4. In the bottom of Table V are listed the percent contributions from W_2^{6+} fragment orbitals in the $16b_u$ and $17b_u$ orbitals of $W_4(OH)_{12}$ for selected points along the reaction coordinate. The first point germane to the above question is that the $16b_u$ orbital has virtually no contribution from either the π_g or δ_g orbitals of W_2^{6+} at any point along the reaction coordinate. Instead, the $16b_u$ orbital starts out (point I) as a mixture of occupied σ_g and π_u orbitals and simply increases in the percent π_u contribution until at the final point (F) it corresponds to the metal–metal π bonds of isolated $W_2(OH)_6$ fragments (compare to the $5e_u$ orbital of Table IV). If this is an avoided crossing between π_u and π_g orbitals like that seen for cyclobutadiene, then we should expect to see the memory (or intent) of this crossing revealed in the W_2^{6+} percent characters just as we saw for the

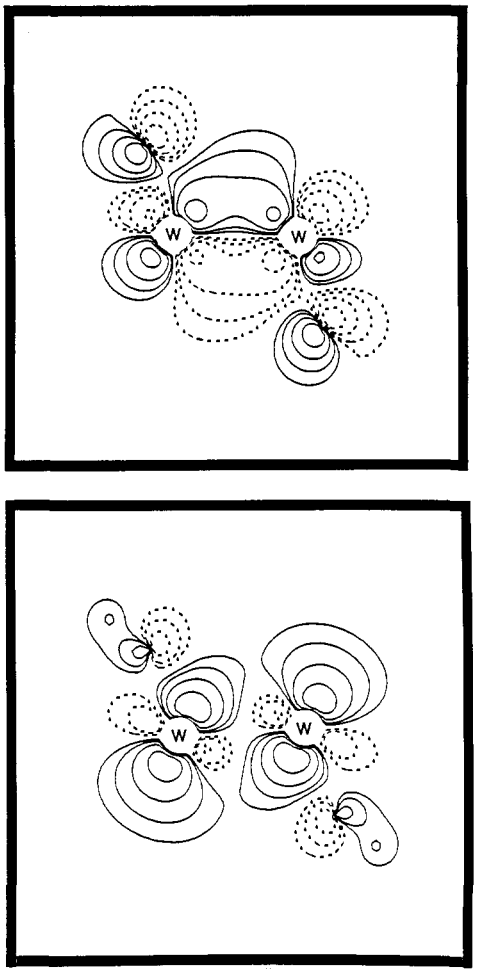

Figure 16. Contour plots comparing the $5e_u$ (top) and $5e_g$ (bottom) orbitals of $W_2(OH)_6$. These plots are taken in a plane containing the two W atoms and two terminal oxygen and hydrogen atoms of the OH ligands. Positive and negative contour values are indicated by solid and dashed lines, respectively. Contour values begin at ±0.02 e/Å^3 and increase by a factor of 2 at each step.

Table V. Percent Contribution from W_2^{6+} Fragment Oribtals in Relevant Molecular Orbitals of $W_4(OH)_{12}$ at Selected Points Along the C_{2h} Reaction Coordinate

	$15a_g$					$16a_g$				
	I	2	4	6	F	I	2	4	6	F
σ_g	1	0	45	65	75	51	58	15	1	0
π_u	22	27	13	1	0	0	0	35	60	66
δ_g	6	8	0	0	0	6	2	4	2	0
δ_u	3	3	0	1	0	0	2	7	2	1
π_g	0	0	0	0	0	5	2	0	0	0
σ_u	3	3	0	1	0	0	0	4	0	0
6_s	25	22	18	10	19	1	2	2	1	0
6_p	8	9	3	0	0	0	0	5	2	4
	$16b_1$					$17b_1$				
	I	2	4	6	F	I	2	4	5	F
σ_g	22	16	1	5	0	4	3	1	0	0
π_u	25	37	68	65	66	6	3	0	0	0
δ_g	4	1	0	0	0	25	42	44	37	45
δ_u	1	0	0	3	1	21	0	11	13	0
π_g	0	1	0	2	0	5	0	3	8	33
σ_u	8	7	1	1	0	9	22	18	14	0
6_s	0	1	0	0	0	0	3	0	6	0
6_p	0	0	0	0	4	4	1	2	2	0

(26) Bursten, B.; Cotton, F. A.; Green, J. C.; Seddon, E. A.; Stanley, G. G. *J. Am. Chem. Soc.* **1980**, *102*, 4579.
(27) Chisholm, M. H.; Clark, D. L.; Kober, E. M.; Van Der Sluys, W. G. *Polyhedron* **1987**, *6*, 723.
(28) Hopkins, M. D.; Gray, H. B.; Miskowski, V. M. *Polyhedron* **1987**, *6*, 705 and references therein.

$15a_g$–$16a_g$ crossing noted above and the $4b_u$–$5b_u$ crossing in C_4H_4. Notice that the π_g contribution to this orbital is virtually nonexistent at any point along the reaction coordinate. It is concluded, therefore, that the occupied $16b_u$ orbital of $W_4(OH)_{12}$ has no memory of there ever being a crossing, avoided or otherwise!

Let us now examine the unoccupied $17b_u$ orbital for there are some rather peculiar things happening. At the initial point (I) the unoccupied $17b_u$ orbital is an admixture of predominantly δ_g and δ_u character of W_2^{6+}. We also see a small percentage of σ_g, π_u, π_g, and σ_u character. Recall that for separated $W_2(OH)_6$ molecules the metal–metal π bond is composed of 66% π_u and only 1% δ_u character (see points marked F, or Table IV). Similarly, the metal–metal π^* orbital is composed of 45% δ_g and 33% π_g character. Thus as we follow the $17b_u$ orbital from point I to F along the reaction coordinate, we recognize the δ_g and π_g character as representing the metal–metal π^* orbitals of separated $W_2(OH)_6$. Similarly, the lack of π_u character implies no memory (or at least a severe case of amnesia) of an avoided crossing between π and π^* orbitals. Recall that the occupied metal–metal π bond is 66% π_u in character with a mere 1% δ_u character. Accordingly, the δ_u character represents, instead, a contribution from metal–ligand bonding that helps to lessen the metal–metal antibonding in the $17b_u$ orbital. In spite of the complications with the antibonding $17b_u$ orbital, the lack of π_g and δ_g contribution to the occupied $16b_u$ orbital is strong evidence in support of the original suggestion that the concerted dimerization of $W_2(OH)_6$ is a symmetry-allowed process. Furthermore, the use of a diatomic "memory probe" does a good job of revealing the intent of two orbitals to cross as illustrated for the b_u crossing of C_4H_4 as well as the a_g crossing in $W_4(OH)_{12}$.

Presumably, the difference between the "allowedness" of the C_2H_2 and $W_2(OR)_6$ dimerization reactions lies in the nature of the π^* orbitals. If the y axis is defined in the plane of the paper, then C–C π and π^* orbitals may be constructed from pure p_y atomic orbitals on carbon as shown qualitatively in VI. A

VI

misconception about the π and π^* orbitals of $W_2(OR)_6$ is that they can be constructed from pure d_{yz} atomic orbitals as in the quadruply bonded systems such as $W_2(O_2CR)_4$ where a C_4 axis is maintained. This is shown qualitatively in VII. This is ob-

VII

viously not right, because the presence of a C_3 axis allows for the mixing of d_{yz} and $d_{x^2-y^2}$ atomic orbitals, i.e., a mixing of δ and π character. The contour plot of the π^* orbital of $W_2(OH)_6$ shown in Figure 16 illustrates this phenomenon. The effect of the δ_g mixing in the π^* orbital is to help lessen the degree of metal–metal antibonding and this is illustrated qualitatively in VIII. The in-phase (b_u) combination of two pure π^* orbitals (VIII, left) appears to give rise to a bonding orbital as shown qualitatively on the left of IX. This of course is what makes the C_2H_2 di-

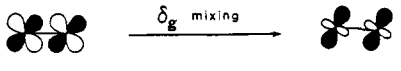

VIII

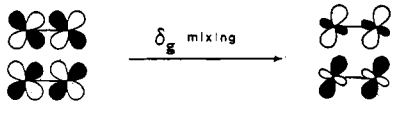

IX

merization forbidden. By contrast, if we allow the δ_g mixing, we see that our proposed bonding orbital (IX, left) is actually antibonding! This is shown on the right of IX. This behavior is clearly not possible for the π^* orbitals of C_2H_2 and illustrates the added flexibility of d-orbitals in this system.

This observation raises one further question regarding the a_g combination of π^* orbitals which could now be bonding after inclusion of δ_g mixing. This would show up as an avoided crossing between the occupied $16a_g$ and unoccupied $17a_g$ orbitals in the Walsh diagram. Suffice it to say, that such a crossing would be revealed in the diatomic probe and it is not. Note that Table V shows little evidence of δ_g and π_g character in the $16a_g$ orbital. Similarly, the $17a_g$ orbital (not shown in Table V) starts out as 55% π_g and mixes with δ_g character along the reaction coordinate.

Concluding Remarks

This work provides the first observation of the interconversion of two M–M triply bonded compounds and their dimeric, 12-electron cluster. The following aspects of the work represent significant discoveries within this context and provide impetus for future studies.

1. The dynamics of the $W_4(O\text{-}i\text{-}Pr)_{12}$ molecule are most fascinating. The cluster oscillates about a symmetric M_4 rhombus such that the central W_4O_{12} moiety has time-averaged D_{2h} symmetry. This interconverts the M–M double and single bonds. Correlated with this motion of the central $W_4(\mu\text{-}O)_4$ moiety is a proximal $\rightleftarrows$ distal exchange of the terminal O-*i*-Pr ligands associated with the wingtip tungsten atoms. The combined motions are termed the *Bloomington Shuffle* as depicted in Figure 4. The analogy with cyclobutadiene is again striking. According to the best calculations, C_4H_4 should adopt a rectangular geometry, and double bond flipping can take place via a square transition state with a rhomboidal transition state at still higher energy.[4] Both clusters, $W_4(O\text{-}i\text{-}Pr)_{12}$ and C_4H_4, avoid the square ground state due to second-order Jahn–Teller effects, yet why the inorganic system should prefer to adopt the distorted ground state rather than a rectangular one is not obvious, though clearly the presence of d orbitals allows for a bonding interaction between the backbone W atoms in the rhombus.

2. The combined operations of the *Bloomington Shuffle* together with equilibrium 1 provide a metathesis of tungsten atoms in the W≡W bonds. Such a metathesis can be investigated by mass spectroscopy with the use of specific isotopic labeling experiments involving $^{18x}W_2(O\text{-}i\text{-}Pr)_6$ and the natural abundance $W_2(O\text{-}i\text{-}Pr)_6$. Hopefully the necessary tungsten isotopes will be avilable to us at reasonable cost so that this experiment may be carried out.

3. The thermodynamic parameters for equilibrium 1 show that while the cluster is enthalpically favored, a significant sacrifice in entropy is involved, −61 eu.[29] Activation parameters for the coupling of two $W_2(O\text{-}i\text{-}Pr)_6$ units require a highly ordered transition state, one approaching the order of the product. In this regard an analogy can be made to so-called concerted organic reactions such as the Diels–Alder reaction.

4. An analysis of the interconversion of $W_4(\mu\text{-}OH)_4(OH)_8$ and two $W_2(OH)_6$(M≡M) units indicates that this, unlike its organic counterpart $C_4H_4 \rightleftarrows 2C_2H_2$, is a symmetry-allowed reaction in the Woodward–Hoffmann sense. Of course, unlike organic reactions involving only C–C bond formation, in the inorganic coupling of two W≡W units the alkoxide groups make the initial contact, i.e., alkoxide bridge formation occurs prior to any significant M···M bond formation.

5. Finally, and undoubtedly most significantly, this work opens the door to studies of the reactivity of $W_2(OR)_6$(M≡M) compounds and their 12-electron cluster $W_4(OR)_{12}$ compounds. It appears that the stability of the $W_4(OR)_{12}$ species depends upon the steric pressure at the metal center while the kinetic barrier to the dimerization of two $W_2(OR)_6$ molecules is dependent on

(29) Similar thermodynamic parameters have been evaluated from a $^1H\{^{119}Sn\}$ double resonance NMR study of the dimer–tetramer equilibrium involving $[MeSn(OR)_3]_x$ compounds, $x = 2$ and 4: see ref 17.

the accessibility of the oxygen atoms to W–μ-OR bond formation. Thus, $W_2(ONp)_6$, where Np = neopentyl, dimerizes roughly 100 times slower than $W_2(O\text{-}i\text{-}Pr)_6$ though the cluster $W_4(ONp)_{12}$, once formed, does not dissociate in toluene-d_8 even at +80 °C.[14] The large energy of activation for the coupling of two $W_2(O\text{-}i\text{-}Pr)_6$ units allows a trivial synthesis of the pure dinuclear compound (see Experimental Section). The addition of *i*-PrOH (excess) to a hydrocarbon solution of $W_2(O\text{-}t\text{-}Bu)_6$ at −78 °C leads to rapid alcoholysis and at this temperature the $W_2(O\text{-}i\text{-}Pr)_6$ molecule is effectively inert to cluster formation.

Never before in chemistry have we had the opportunity to compare the reactivity of an E–E multiple bond and its dimer E_4 separately, under mild and amenable experimental conditions, i.e., not in a matrix or ion beam experiment. Already this has led us to observe the C–C and C–H bond activation of ethylene by the unligated compounds $W_2(OR)_6$ where R = *i*-Pr and Np.[10,11]

Experimental Section

Syntheses. All reactions were carried out under an atmosphere of dry and oxygen-free nitrogen with standard Schlenk and glovebox techniques. Hydrocarbon solvents were freshly distilled from sodium benzophenone ketyl before use. $W_4(O\text{-}i\text{-}Pr)_{12}$ was prepared as described previously.[1] $W_2(O\text{-}i\text{-}Pr)_6$ used for kinetic measurements was prepared according to the procedure described below so that any possible contamination with NMe_3, from the synthesis in the previous paper,[1] could be ruled out.

$W_2(O\text{-}i\text{-}Pr)_6$. Typically 0.500 g (0.62 mmol) of $W_2(O\text{-}t\text{-}Bu)_6$ was dissolved in 8 mL of hexane at room temperature. The solution was cooled to −78 °C in a dry ice–acetone bath, precipitating some $W_2(O\text{-}t\text{-}Bu)_6$. Dry isopropyl alcohol (1.5 mL) was added slowly and the solution slowly changed color from orange-red to bright yellow with a pale yellow precipitate. The mixture was stirred for 2 h after which $W_2(O\text{-}i\text{-}Pr)_6$ was isolated by filtration at −78 °C, in virtually quantitative yield.

Equilibrium and Rate Constant Measurements. The equilibrium constants, K_{eq}, and rate constants have been measured for the equilibrium

$$W_4(O\text{-}i\text{-}Pr)_{12} \underset{k_{-1}}{\overset{k_1}{\rightleftharpoons}} 2W_2(O\text{-}i\text{-}Pr)_6$$

for both the forward, k_1, and reverse, k_{-1}, reactions, where $K_{eq} = k_1/k_{-1}$ and $K_{eq}^{-1} = k_{-1}/k_1$ (see Table I).

(i) **Preparation of Samples.** Both equilibrium constants and rate constants were measured by comparison of the integral ratios of the methine protons of $W_4(O\text{-}i\text{-}Pr)_{12}$ and $W_2(O\text{-}i\text{-}Pr)_6$ by ^1H NMR spectroscopy from solutions of known concentrations. The solid samples were weighed (±0.5 mg) into 5-mm NMR tubes and an accurately measured volume of solvent (toluene-d_8) (±20 μL) was added under N_2 at liquid nitrogen temperature. The samples were sealed in vacuo and kept frozen until they were completely dissolved at the desired temperature and quickly placed in the pre-equilibrated NMR probe. All ^1H NMR data were obtained with a Nicolet NT-360 instrument and temperatures were calibrated with ethylene glycol or methanol standards where appropriate. ^1H NMR spectra were referenced to the protio impurity of the methyl resonance of toluene-d_8. The concentration of a saturated solution of $W_4(O\text{-}i\text{-}Pr)_{12}$ in toluene-d_8 is approximately 0.08 M at 26.5 °C. The plot of ln K_{eq} vs $1/T$ yielded the ground-state thermodynamic parameters given in Table I. The values of k_1 determined in this manner are given in Table I. Although it is possible to calculate k_{-1} from these results and so calculate the activation parameters for the reverse (associative) process, we also measured k_{-1} directly by conducting similar experiments starting with pure $W_2(O\text{-}i\text{-}Pr)_6$. The measured values of the second-order rate constant k_{-1} and measured equilibrium constants K_{eq}^{-1} (where $K_{eq}^{-1} = (K_{eq})^{-1}$) are given in Table I together with the derived activation parameters. By plotting the concentration of $W_4(O\text{-}i\text{-}Pr)_{12}$ and $W_2(O\text{-}i\text{-}Pr)_6$ against time smooth curves were obtained, which indicates that no other species are formed during the approach to equilibrium.

(ii) **Equilibrium Constants.** The equilibrium constants were measured in the temperature range 23 to 44 °C at a concentration of 0.0277 M by allowing samples containing pure $W_4(O\text{-}i\text{-}Pr)_{12}$ to equilibrate in constant temperature baths. The individual concentrations of $W_4(O\text{-}i\text{-}Pr)_{12}$ and $W_2(O\text{-}i\text{-}Pr)_6$ were measured by ^1H NMR by comparison of integral ratios of the sharp methine septet of $W_4(O\text{-}i\text{-}Pr)_{12}$ (representing one-third of its total concentration) with that due to $W_2(O\text{-}i\text{-}Pr)_6$. The relationship between the concentrations and K^1_{eq} is given below and the data are tabulated in Table I.

$$K_{eq} = [W_2(O\text{-}i\text{-}Pr)_6]^2/[W_4(O\text{-}i\text{-}Pr)_{12}]$$

(iii) **Rate Constants.** The rate constant, k_1, for the dissociation of $W_4(O\text{-}i\text{-}Pr)_{12}$ was measured at six different temperatures in the range +23 to +44 °C at a concentration of 0.0277 M. The rate constant, k_{-1}, for the association of two $W_2(O\text{-}i\text{-}Pr)_6$ molecules was measured at six different temperatures and at a concentration of 0.0554 M (0.0277 M in $W_4(O\text{-}i\text{-}Pr)_{12}$). The approach to equilibrium was followed for 4–5 half-lives or until equilibrium was established (at higher temperatures) by ^1H NMR spectroscopy with the Nicolet kinetics program. The final concentrations of the $W_4(O\text{-}i\text{-}Pr)_{12}$ and $W_2(O\text{-}i\text{-}Pr)_6$ species at equilibrium were taken at least 20 h later. A portion of a typical experiment is shown in Figure 6. The individual concentrations of $W_4(O\text{-}i\text{-}Pr)_{12}$ and $W_2(O\text{-}i\text{-}Pr)_6$ for each set of experimental conditions (temperature and concentration) were treated according to reversible first- and second-order kinetics.

For the unimolecular direction

$$A \underset{k_{-1}}{\overset{k_1}{\rightleftharpoons}} 2B$$

time = 0	$[A_0]$	0
time = t	$([A_0] - x)$	$2x$
time = equilib	$([A_0] - x_e)$	$2x_e$

$$k_1 = \frac{x_e}{(2[A_0] - x_e)t} \ln\left[\frac{[A_0]x_e + x([A_0] - x_e)}{[A_0](x_e - x)}\right]$$

For the bimolecular direction

$$2B \underset{k_1}{\overset{k_{-1}}{\rightleftharpoons}} A$$

time = 0	$[B_0]$	0
time = t	$(B_0 - 2x)$	x
time = equilib	$(B_0 - 2x_e)$	x_e

$$k_1 = \frac{x_e}{([B_0]^2 - 4x_e^2)t} \ln\left[\frac{x_e([B_0]^2 - 4x_e x)}{[B_0]^2(x_e - x)}\right]$$

These expressions may be further simplified in terms of A/A_0 and A/A_e and the rate constants were determined with a program written by Dr. J. J. Gajewski.

Computational Procedures. The coordinates for the model compound of formula $W_4(OH)_{12}$ were idealized to C_{2h} point symmetry, but otherwise bond lengths and angles were taken from the crystal structure of $W_4(O\text{-}i\text{-}Pr)_{12}$ reported in the previous paper.[1] The W–W distances used were 2.502, 2.732, and 2.807 Å for the "short", "long", and "backbone" W–W distances (as described in the previous paper), respectively.[1] The terminal W–O distances were set at the average value of 1.891 Å to maintain C_{2h} symmetry. The O–H distances were assumed to be 0.96 Å.

The coordinates for the dinuclear model of formula $W_2(OH)_6$ were idealized to D_{3d} point symmetry, but otherwise bond lengths and angles were taken from the crystal structure of $W_2(O\text{-}i\text{-}Pr)_6$.[1] Two sets of structural parameters were generated. The first set, idealized from the crystal structure, used W–W, W–O, and O–H distances of 2.315, 1.880, and 0.96 Å, respectively, and a W–W–O angle of 107°. The second set, used in constructing the Walsh diagram, used W–W and W–O distances of 2.502 and 1.891 Å, respectively, while the W–W–O angle and O–H distance were as stated above.

The reaction coordinate for the Walsh diagram consists of 11 separate calculations. The origin on the $W_4(OH)_{12}$ side was taken to be the idealized C_{2h} $W_4(OH)_{12}$ calculation. From this origin the reaction coordinate consists of 9 synchronous regular variations of W–W–O bond angles and the diagonal W–W distances while maintaining C_{2h} symmetry throughout. This amounts to pulling a parallelogram of W atoms apart while maintaining two parallel edges. The "short" W–W distance was held constant at 2.502 Å, and the W–O distances and W–O–H angles were held constant throughout the reaction coordinate. This rudimentary procedure allowed the hydrogen atoms to follow closely and automatically the W–W–O angle changes, and hence the cycloreversion process. The final calculation on the $W_2(OH)_6$ side of the reaction coordinate consists of two $W_2(OH)_6$ molecules (W–W = 2.502 Å) arranged with overall C_{2h} symmetry. The local symmetry about each $W_2(OH)_6$ center was D_{3d} with the closest W–W distance (along the diagonal) between dinuclear centers fixed at 6.0 Å.

Molecular orbital calculations were performed with the approximate, nonempirical LCAO method of Fenske and Hall which has been described in detail elsewhere.[21] All calculations reported here were obtained at the Indiana University Computational Chemistry Center with a VAX 11/780 computer system. Contour plots were generated on a TALARIS 800 laser printer with solid lines representing positive density contours and dashed lines representing negative density contours.

Slater atomic orbital bases were obtained by optimally fitting the numerical Herman–Skillman radial functions[30] with Slater-type orbitals

(STOs) using the method of Bursten, Jensen, and Fenske.[31] Contracted double-ζ representations were constructed for the W 5d and O 2p, while single-ζ representations were used for all other orbitals. Valence AOs were orthogonalized to all other valence and core orbitals of the same atom. Basis functions for the W atom were derived for a +1 oxidation state with the 6s and 6p exponents fixed at 1.8. An exponent of 1.16 was used for the H 1s atomic orbital.[32]

Acknowledgment. We thank the National Science Foundation for support. D.L.C. was the Indiana University General Electric Fellow 1985-86. We thank Professors E. R. Davidson, J. J. Gajewski, L. K. Montgomery, and R. Hoffmann for stimulating discussions.

Registry No. $W_2(O\text{-}i\text{-}Pr)_6$, 71391-16-7; $W_4(O\text{-}i\text{-}Pr)_{12}$, 104911-26-4.

(30) Herman, F.; Skillman, S. *Atomic Structure Calculations*; Prentice-Hall: Englewood Cliffs, NJ, 1963.
(31) Bursten, B. E.; Jensen, J. R.; Fenske, R. F. *J. Chem. Phys.* **1978**, *68*, 3320.
(32) Hehre, W. J.; Steward, R. F.; Pople, J. A. *J. Chem. Phys.* **1969**, *51*, 2657.

Heteropolyvanadates Containing Two and Three Manganese(IV) Ions: Unusual Structural Features of $Mn_2V_{22}O_{64}^{10-}$ and $Mn_3V_{12}O_{40}H_3^{5-}$

Hikaru Ichida,[1] Kenji Nagai,[1] Yukiyoshi Sasaki,*[,1] and Michael T. Pope*[,2]

Contribution from the Departments of Chemistry, University of Tokyo, Hongo, Tokyo 113, Japan, and Georgetown University, Washington, D.C. 20057. *Received May 12, 1988*

Abstract: The crystal structures of the vanadomanganate(IV) salts $K_{10}Mn_2V_{22}O_{64}\cdot 20H_2O$ (**1**) and $K_5H_3Mn_3V_{12}O_{40}\cdot 8H_2O$ (**2**) are reported. Compound **1** is triclinic, space group, $P\bar{1}$; a = 15.710 (4) Å, b = 12.671 (4) Å, c = 10.281 (3) Å; α = 113.62 (2)°, β = 92.56 (3)°, γ = 79.54 (3)°; Z = 1. The heteropolyanion consists of a centrosymmetric arrangement of two MnV_{11} moieties linked by two linear unsupported V–O–V bridges. Each MnV_{11} unit comprises edge-shared MO_6 octahedra and may be regarded as a manganese-substituted decavanadate structure with two additional VO_6 octahedra that contribute to the bridging section of the whole structure. The V–O bond lengths in the bridges (1.779 Å) imply bond orders of unity, and the heteropolyanion may therefore be regarded as a double "anhydride", $[(MnV_{11}O_{31})_2O_2]^{10-}$ (compare $[(C_9H_6NO)VO]_2O$ and $[(Nb_2W_4O_{18})_2O]^{2-}$). Other bond lengths and angles are unexceptional. Compound **2** is triclinic, space group, $P\bar{1}$; a = 11.800 (2) Å, b = 16.555 (2) Å, c = 11.267 (20) Å; α = 102.91 (1)°, β = 109.48 (1)°, γ = 86.88 (1)°; Z = 2. The anion is a highly condensed edge-shared C_{3v} cluster of MO_6 octahedra based on the arrangement expected for the (unknown) ϵ-isomer of the Keggin structure but with no central "tetrahedral" atom. Instead, MnO_6 octahedra occupy the centers of three of the four faces of the anion. The fourth face has an octahedral vacancy to which the three protons are attached. Although the three MnO_6 octahedra share common edges to form an equilateral triangle of Mn^{4+} cations (Mn···Mn, 2.86–2.88 Å), the anion shows virtually no magnetic coupling (J = −0.3 cm^{-1}) based upon susceptibility measurements to 10 K.

There is considerable current interest in the chemistry and structures of polyoxoanions of the early transition elements vanadium, molybdenum, and tungsten in view of their perceived importance in catalysts.[3] Because of the different oxidation state and stereochemical preferences of vanadium compared with molybdenum and tungsten, there is no reason to expect that the structures (or indeed the stoichiometries) of the vanadates would be similar to those of the molybdates and tungstates. However,

Table I. Crystal Data for **1**

formula	$K_{10}Mn_2V_{22}O_{64}\cdot 20H_2O$
formula wt	3005.8
crystal system	triclinic
space group	$P\bar{1}$
a, b, c (Å)	15.710 (4), 12.671 (4), 10.281 (3)
α, β, γ (deg)	113.62 (2), 92.56 (3), 79.54 (3)
cell volume	1843 (1) Å^3
Z	1
density (g·cm^{-3})	2.67 (calcd), 2.64 (obsd)
μ (Mo Kα)	3.53 mm^{-1}
F(000)	1358
temp	298 K
$(\sin\theta/\lambda)_{max}$	0.7035 Å^{-1}
hkl range	$-20 \le h \le 22$, $0 \le k \le 17$, $-14 \le l \le 14$
no. reflcns	11287; 8085 ($\lvert F_o\rvert > 3.0\sigma(\lvert F_o\rvert)$)
scan mode	ω–2θ
scan speed	4° min^{-1} (ω)
$\Delta\omega$	1.0 + 0.5 tan θ
R	0.067
R_w	0.100, $w^{-1} = \sigma^2(\lvert F_o\rvert) + (0.01\lvert F_o\rvert)^2$
$(\Delta/\sigma)_{max}$	0.2
$\Delta\rho/e$ Å^{-3}	<1.8

(1) Tokyo University.
(2) Georgetown University.
(3) Research activity is high in this area and has not been comprehensively reviewed recently. The following lists recent papers from some different research groups (alphabetically by first author) that are currently active and provides an entree to the literature. (a) Ai, M. *Polyhedron* **1986**, *5*, 103. (b) Akid, R.; Darwent, J. R. *J. Chem. Soc., Dalton Trans.* **1986**, 395. (c) Aoshima, A.; Yamaguchi, T. *Nippon Kagaku Kaishi* **1986**, 1161. (d) Baba, T.; Ono, Y. *J. Mol. Catal.* **1986**, *37*, 317. (e) Dun, J. W.; Gulari, E.; Streusand, B. *Appl. Catal.* **1986**, *21*, 61. (f) Finkė, R. G.; Rapko, B.; Domaille, P. J. *Organometallics* **1986**, *5*, 175. (g) Fox, M. A.; Cardona, R.; Gillard, E. *J. Am. Chem. Soc.* **1987**, *109*, 6347. (h) Hill, C. L.; Brown, R. B., Jr. *J. Am. Chem. Soc.* **1986**, *108*, 536. (i) Kulikov, S. M.; Kozhevnikov, I. I.; Fomina, M. N.; Krysin, A. P. *Izv. Acad. Nauk SSSR, Ser. Khim.* **1988**, 752. (j) Misono, M.; Okahara, T.; Ichiki, T.; Arai, T.; Kanda, Y. *J. Am. Chem. Soc.* **1987**, *109*, 5535. (k) Moffat, J. B. *Stud. Surf. Sci. Catal.* **1987**, *31*, 241. (l) Nomiya, K.; Sugie, Y.; Miyazaki, T.; Miwa M. *Polyhedron* **1986**, *5*, 1267. (m) Papaconstantinou, E.; Argitis, P.; Dimotikali, D.; Hiskia, A.; Ionnidis, A. *NATO ASI Ser., Ser. C* **1986**, *174*, 415. (n) Siedle, A. R.; Markell, C. G.; Lyon, P. A.; Hodgson, K. O.; Roe, A. L. *Inorg. Chem.* **1987**, *26*, 219. (o) Urabe, K.; Tanaka, Y.; Izumi, Y. *Chem. Lett.* **1985**, 1595. (p) Vasilevskis, J.; De Deken, J. C.; Saxton, R. J.; Wentreck, P. R.; Fellmann, J. R.; Kipnis, L. S. PCT Int. Appl. WO 01,615 [*Chem. Abstr.* **1987**, *107*, 178602p]. (q) Venturello, C.; D'Aloisio, R.; Bart, J. C. J.; Ricci, M. *J. Mol. Catal.* **1985**, *32*, 107. (r) Yamase, T.; Watanabe, R. *J. Chem. Soc., Dalton Trans.* **1986**, 1669.

0002-7863/89/1511-0586$01.50/0